Chapter 4

Photometric Observations

Abstract:

The photometric data of a sample of disk galaxies from the Eridanus group are presented in the optical R-band, and near-infrared J, H, and K bands. The optical R-band observations are from the 1-m reflector at State Observatory, Nainital, India. The near-infrared data is from the *Two Micron All Sky Survey (2MASS)*. The R-band images are sensitive down to a surface brightness of 26.5 mag arcsec^{-2}. The $2MASS$ images have the limiting sensitivity of 21 mag arcsec^{-2} in the J band, and 20 mag arcsec^{-2} in the K band. The axial parameters (position angle, and ellipticity) of the disk, surface brightness profiles in different bands, color profiles, total magnitudes, central disk surface brightnesses, and disk scale lengths of galaxies are estimated using the data from all the bands. A correlation between the disk scale length and the central disk surface brightness is noticed. The central disk surface brightness is also weakly correlated with the galaxy type in the sense that the early type galaxies have brighter central surface brightnesses than the late type galaxies. This data along with the H I data from GMRT will be used to construct the Tully-Fisher relations.

Keywords: Photometry, central disk surface brightness, disk scale length

4.1 Introduction

In this chapter, R-band and near-infrared (near-IR) J, H, and K band photometric data on the Eridanus group of galaxies are presented. The R-band images are obtained from the CCD observations using the 1-m optical telescope at the State Observatory (SO), Nainital and the J, H, and K band CCD images are obtained from the *Two Micron All Sky Survey (2MASS)*. These data will be used to make a comparison between the H I and the optical properties of galaxies, and, to construct the Tully-Fisher (T-F) relations. The near-IR images, least affected by internal dust extinction in galaxies, provide better estimate of the total luminosity. The sensitivity to detect radiation in the near-IR bands is, however, poorer than in the optical bands mainly due to the increased sky background in the near-infrared bands. The night sky is brighter by ~ 5 magnitude in the J band and about ~ 7 magnitude in the K band as compared to the B-band. The near-IR images obtained with moderate integration times ($10 - 20$min.) on telescopes of moderate sizes (1-m) will not be sensitive to detect the fainter outer regions of galaxies. But, it is still possible to get an estimate of the missing light in spirals by extrapolating the disk light profiles which obey a well defined exponential law as a function of the galactocentric distance. The R-band observations on the other hand, are still useful as low surface brightness outer regions of the stellar disks can be traced easily with moderate integration time ($10 - 20$min.) on telescopes of moderate sizes (1-m). Also, the dust extinction would not completely obscure galaxies in the R-band.

There is another advantage in using the near-infrared data. The light in the near-IR bands come mainly from the old stellar population (cool red giants) which is the dominant visible mass component of a galaxy. Hence, the near-IR light traces the underlying galactic potential due to the stellar component. The stellar mass to light ratios in the near-IR bands are least affected by the recent star formation history (Bell & de Jong 2000). The near-IR imaging of galaxies are, therefore, crucial for studies like TF relations, dynamical properties of galaxies, and dark matter halos.

4.2 R-band Observations and data analyses

The Telescope The broad band $Cousins - R$ ($\lambda_{eff} = 0.65$ μm, BW= 0.22 μm) photometric obser-

Table 4.1: R-band observations

Name	Date of Obs. (mm-dd-yyyy)	# of frames	Exp. time (min.)	Airmass	FWHM ($''$)
NGC 1385	11-10-2002	6	30	1.65	2.7
IC 1953	11-10-2002	4	20	1.87	2.9
NGC 1359	11-10-2002	3	15	2.07	3.6
NGC 1309	12-10-2002	3	15	1.58	2.2
NGC 1325	12-10-2002	2	10	1.66	2.6
NGC 1367	12-10-2002	3	15	1.66	3.2
SGC 0321.2-1929	13-10-2002	2	30	1.54	2.0
ESO 548- G 065	13-10-2002	2	10	1.57	2.6
NGC 1347	13-10-2002	2	10	1.59	2.9
IC 1952	13-10-2002	3	10	1.66	2.3
NGC 1414	13-10-2002	2	10	1.68	2.9
NGC 1422	13-10-2002	2	10	1.68	2.9
ESO 482- G 035	13-10-2002	2	10	1.71	2.8
MCG -03-10-041	13-10-2002	2	10	1.76	3.1
ESO 548- G 005	13-10-2002	2	10	1.77	3.6
ESO 482- G 013	13-10-2002	3	15	1.83	2.8
IC 1962	13-10-2002	3	15	1.87	2.4
ESO 548- G 025	15-10-2002	2	10	1.59	3.0
NGC 1345	15-10-2002	2	10	1.63	2.1
ESO 549- G 018	15-10-2002	2	10	1.64	2.4
ESO 549- G 002	15-10-2002	2	10	1.95	2.8
ESO 548- G 032	17-10-2002	2	10	1.59	3.1
NGC 1390	17-10-2002	2	10	1.83	3.8
NGC 1415	17-10-2002	3	9	2.04	3.5

vations of 26 galaxies in the Eridanus group were carried out during October, 11 – 15, 2002 using the 1-m Sampurnanand reflector of the State Observatory (longitude $79^o27'$ E, latitude $29^o22'$ N, altitude 1955 m.) located in the Himalayan region near Nainital, India. This telescope uses the Ritchey-Chrétien system with a f/13 Cassegrain focus. The diameter of the secondary mirror is 32.4 cm with the distance between the primary and the secondary being ∼2.92 m. This configuration provides a plate scale of $15''.5$/mm.

The Detector The data were recorded on to 2048×2048 pixels TekCCD camera cooled at the temperature of liquid Nitrogen ($-110°$ C). The CCD covers a field of view $\sim 13' \times 13'$ on the sky with each square element having a resolution of $0''.38 \times 0''.38$. The data were acquired after averaging the counts in every 2×2 pixels making each square element equal to $0''.76 \times 0''.76$. The read-out noise and gain of the CCD camera are 10 e^- and 5.3 e^- per analog-to-digital count respectively. Two to five frames each of 5 min or 3 min duration were observed for each galaxy. A few low surface brightness (LSB) galaxies were observed for a total of 30–60 min duration.

Observational details

The observational parameters are given in Tab. 4.1. The table columns are as follows :

Column 1 : Name of the galaxy.

Column 2 : Date of the R band observations.

Column 3 Number of frames.

Column 4 : Total exposure time in second spent on all the frames.

Column 5 : The mean value of the airmass estimated at the mid-exposure time of the frames.

Column 6 : Seeing ($FWHM$) in arcsecond estimated after co-adding the frames.

Calibration On October 13, 2002 the standard Landolt field SA 92 (Landolt 1992) was observed in the V and R bands for photometric calibration and local atmospheric extinction correction. A total of eight stars from this Landolt field with V magnitudes between 12.5 and 15.6, and, (V–R) colors between 0.31 and 0.72 were observed at different zenith angles. The value of the zero point

is 20.79 ± 0.03 and that of the extinction coefficient (k) is 0.18 ± 0.02 on that night. The value of the color coefficient to make the color correction was insignificant. Hence, no color corrections were made. The typical value for the R-band sky brightness was 20.5 mag arcsec^{-2}. The average seeing was $2''.8 \pm 0''.5$. Based on the vast observing experience at the observatory, if weather is stable during the observing period, no significant variations in the calibration is expected. Hence, the Landolt field was observed during one of the five nights.

Data Reduction On each night of observation, several bias frames were taken and averaged to correct the CCD frames. Since the exposure time in each frame was short, no significant dark counts are expected. Every alternate night, morning twilight flat fields were observed. For the nights when no flat fields were taken, previous day's flat fields were used to correct the images for non-uniformity in the exposure across the field of view. The CCD data reduction was performed using the package *CCDRED* in the *Image Reduction and Analysis facility (IRAF)* software package developed by *National Optical Astronomy Observatory (NOAO)*. The frames were aligned using bright stars in the field. The pixels hit by cosmic rays were removed using the median filtering in each pixel of different frames for a galaxy whenever at least three frames for a field were available. When there were only two frames, the bad pixels were identified by comparing their values with the average in the surrounding pixels. After removing the cosmic ray events, all observed frames for a galaxy were averaged to get the final image. The images were regrided to a pixel size of $1''$. The images were registered for the equatorial coordinates in the J2000 epoch using the *Digitized Sky Survey (DSS)* plates.

The sky background was taken as mode of the distribution of pixel values in the averaged image. If the presence of a bright star near the edge or within the observed frame caused significant light gradients across the frame, or, the electron pickup noise caused bright and dark stripes in the frames, a mean value of the sky was estimated using pixels surrounding the galaxy. The Galactic foreground stars over a galaxy were replaced by an average value of the intensities surrounding the affected region.

Photometric errors The photometric errors arise due to Poisson noise, calibration, sky variations, camera electronics, and flat fielding. The total error can vary in different images depending on sizes and surface brightnesses of galaxies. An error estimate is presented here for a galaxy of diameter $4'$ which is typical sizes of galaxies in the Eridanus group. The light from this model galaxy falls on $\sim$ 78 000 pixels. The statistical uncertainty in the sky subtraction will vary as $\sqrt{\sigma N_{pix}}$. Normally, when the galaxy light is negligible compared to the sky brightness, the Poisson noise will be dominated by the sky background. The standard deviation in the estimates of the average sky brightness is about 3 counts/pixel for the present observations. The error in the sky subtraction will, therefore, be about 485 counts or $\sim$ 14.1 mag. It implies an error of 0.03 mag for a 10 mag galaxy, 0.15 mag for a 12 mag galaxy, and 0.7 mag for a 14 mag galaxy. The additional systematic error may arise due to uncertainties in the calibration which amounts to $\sim$0.05 mag, estimated from the fitting errors in the extinction coefficient and zero-point. Since the weather was stable during the nights of observations, no significant night to night variations in the calibration are expected.

4.3 2MASS J, H, and K band data

The *Two Micron All Sky Survey (2MASS)* is an all sky survey in the near-infrared J (1.24 μm), H (1.66 μm) and K_s (2.16 μm) bands (Jarrett et al. 2000). The 2MASS observations were carried out with two identical 1.3-m telescopes, one at the Whipple Observatory, Arizona for observations of the northern sky, and other at the Cerro Tololo Inter-American Observatory, Chile for observations of the southern sky. Each 2MASS camera consists of a liquid Nitrogen cooled cryostat, housing three 256×256 NICMOS3 CCDs each covering a field of view $8'.5 \times 8'.5$ on the sky with a pixel resolution of $2''.0 \times 2''.0$. The typical seeing was in the range $2''.5$ - $2''.8$. The images in the three bands were obtained simultaneously using beamsplitters. The final calibrated, co-added 6.8s integration time, and full resolution images with $1''.0 \times 1''.0$ sampling are obtained from the 2MASS archive. The factor of two improvement in sampling compared to the pixel size is achieved by dithering.

The overall photometric accuracy of 2MASS images are believed to be $\sim$ 0.1 mag (Jarrett et al. 2000). The zero points are typically 20.9 for the J band, 20.5 for the H band, and 19.9 for the K band. The sky brightnesses are typically 16.0–15.3 mag arcsec^{-2} in the J band, 14.3 mag arcsec^{-2} in the H

band, and 13.5–12.9 mag arcsec^{-2} in the K band. The achieved surface brightness sensitivities (3σ) are $\sim$ 21.0 mag arcsec^{-2} in the J band, $\sim$ 20.5 mag arcsec^{-2} in the H band, and $\sim$ 20.0 mag arcsec^{-2} in the K band.

4.4 Image analyses

The image analyses were carried out using *IRAF*, *KARMA*, and *GIPSY* (*Groningen Image Processing System*). All the images are in the identical format with $1''.0 \times 1''.0$ pixel size and regrided to the J2000 epoch. Foreground stars on galaxies, bad pixels, and other defects in the images were removed and replaced by the mean of pixels surrounding the affected region.

4.4.1 Axial parameters of disks from ellipse fitting

The axial parameters (position angle, and ellipticity) of disks were estimated using the *IRAF* task *ELLIPSE*. The disks of galaxies were fitted with elliptical isophotes of fixed width $2''$ at different radii. The centres of the ellipses was kept fixed at the optical centre of the galaxy. The fitting was carried out only in the R-band images. The inner regions, where often a bar or a bulge is present in galaxies, were excluded during the fit. In highly inclined (inclination $> 70^{\circ}$) galaxies, the presence of a bulge in the centre will affect the axial parameters at all radii. The strong spiral arms and dust lanes can also affect the fitting. To minimize the effects of such patterns in the fitting routine, the annuli were chosen of sufficiently large widths of about $10'' - 20''$ so that such patterns get diluted during the fit. In low inclination galaxies (inclination $< 30^{\circ}$), the position angle is rather poorly determined due to such patterns. In such cases, the position angles were taken from the tilted ring fit to the velocity field described in Chapter 3. The position angles were measured from 0° (North up) to 180° in the anti-clockwise direction. The inclinations (i) were derived from the axial ratio b/a according to Hubble (1926) prescription:

$$cos^2(i) = \frac{q^2 - q_0^2}{1 - q_0^2} \tag{4.1}$$

where $q = (b/a)$ and q_0=0.2 (Holmberg 1946) to account for finite thickness of disks.

4.4.2 Surface brightness profiles, color profiles, scale lengths, and central disk surface brightnesses

The average radial surface brightness in elliptical annuli of width $2''$ were computed as a function of galactocentric radius in all bands using fixed position angle and ellipticity of the disk. The aim of this analysis is to derive the scale length and the central surface brightness of the exponential disk. The position angle and the ellipticity was taken to be identical for all annuli and in all bands. This is to avoid effects of bright spiral arms, and bars on the estimated average surface brightnesses of the disks in different bands. The bars and bulges in galaxies are brighter, but, the spiral arms are fainter in the near infrared bands than in the optical bands. Due to the presence of a bulge or a bar in centres, the surface brightness profiles in the inner regions will deviate from that expected for an exponential disk.

The radial surface brightness profiles ($I(r)$) were fitted by an exponential law ($I(r) = I(0)e^{-r/r_d}$) to estimate the scale length (r_d) and the central disk surface brightness ($I(0)$). Since no bulge was fitted, the inner regions where a bar or a bulge was clearly visible were excluded during the fit. The inner $10''$ region was not included in the fit in any galaxy to avoid the bright nuclear region. Since the spiral arms cause the surface brightness profiles to deviate from an exponential law, such regions were identified visually, and, excluded from the fit. The central disk surface brightness, and surface brightness profiles were converted to magnitudes. The goodness of fit is indicated by the reduced chi-square values in the Tab. 4.2. The radial R–J color profiles were also estimated. The profiles were corrected for the local atmospheric and the Galactic extinction. The values for the Galactic extinction in different bands are taken from Schlegel et al (1998). The histograms of the disk scale lengths in different bands are plotted in Fig 4.1. The maximum scale length in the present sample is $\sim$4.5 kpc.

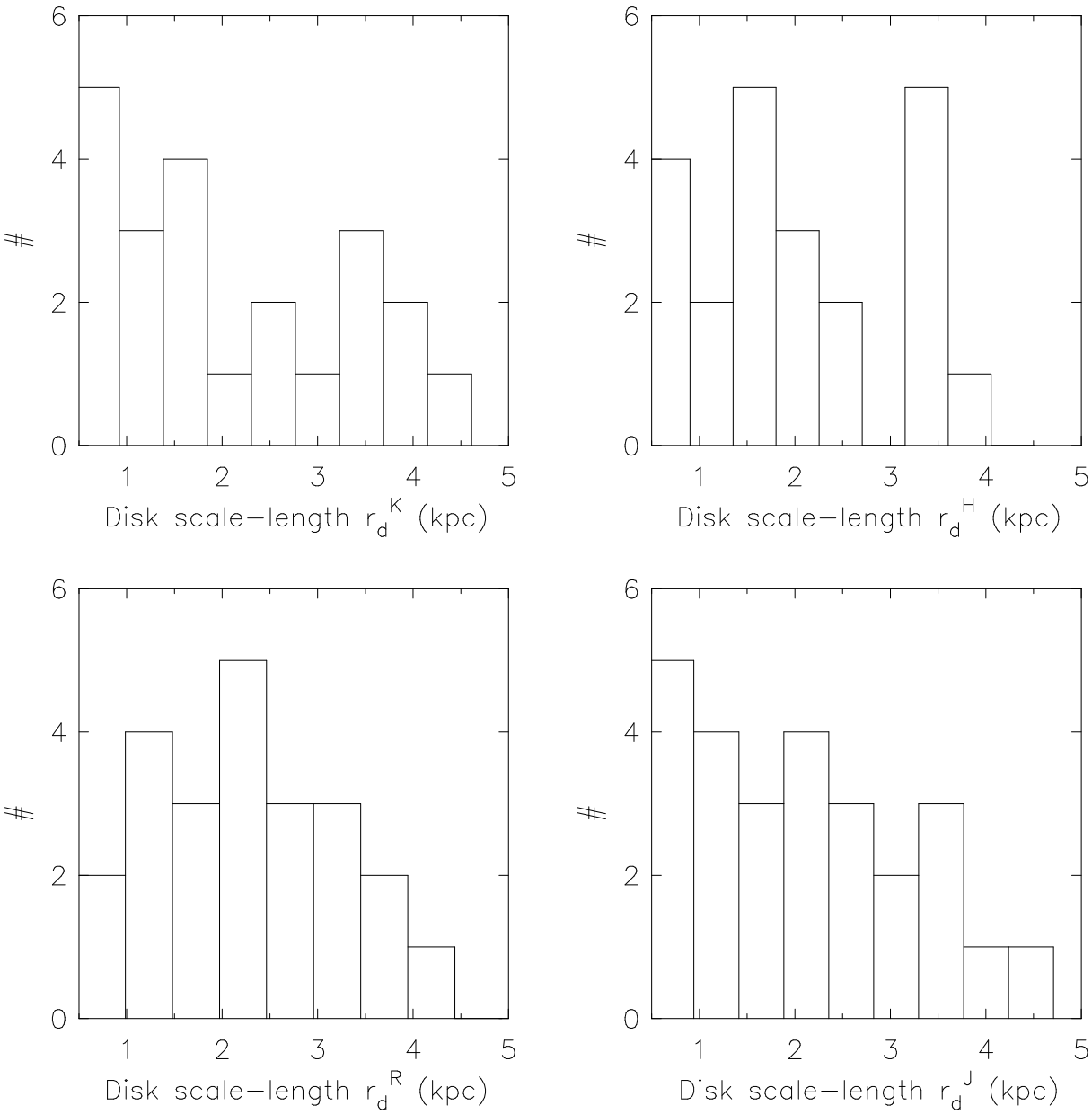

Figure 4.1: Histograms of disk scale lengths in different bands.

4.4.3 Isophotal and total magnitude

The isophotal magnitude m_l^i corrected for the atmospheric extinction is estimated by the following relation:

$$m_l^{iso} = MAGZP - 2.5log(S_l/t) - k.X \tag{4.2}$$

where the subscript l refers to the limiting isophote in a band and the superscript iso refers to isophotal, $MAGZP$ is the zero point magnitude corresponding to 1 second of exposure time, k is the extinction coefficient, X is the airmass, S_l is the total number of counts within the limiting isophote, and t is the total exposure time on the galaxy. The azimuthally averaged limiting surface brightness is 26.0 mag arcsec^{-2} in the R band, 21.0 mag arcsec^{-2} in the J band, 20.5 mag arcsec^{-2} in the H band, and 20.0 mag arcsec^{-2} in the K band. Any observation detects light from galaxies above a certain limiting surface brightness. For instance, in the present case, the near-IR images are sensitive to detect light from galaxies till 2–3 scale lengths, while the R-band images are sensitive up to 4–5 disk scale lengths. The disks could be continuing beyond these limiting radii, and therefore, isophotal magnitudes provide only a lower limit to the total luminosities of galaxies.

It can be shown for an exponential disk that the total light above a certain limiting isophotal radius depends only on the number of scale lengths within that limiting radius, and is given by:

$$\delta m_{ext} = 2.5log\,(1 - (1 + \delta n)exp(-\delta n)) \tag{4.3}$$

(Tully et al. 1996); where δm_{ext} is total light beyond the limiting isophote radius, δn is the number of observed scale lengths within the limiting isophote radius, and is estimated as $(\mu_0 - \mu_{lim}/1.086)$. Where μ_0 and μ_{lim} are the central disk surface brightness and surface brightness of the limiting isophote respectively. These corrections (m_{ext}) are usually large in the near-IR bands as the number of observed scale lengths are less in the near-IR bands compared to the optical bands. Tully et al. (1997) suggested that the disks finally truncate at large radii, and therefore, the correction given by Equ. 4.3 overestimates the light. They advocated for only 88% of δm_{ext} given by Equ. 4.3 as a correction factor. The $0.88\delta m_{ext}$ combined with the isophotal magnitude gives total magnitude.

4.4.4 Extinction corrections

Total magnitudes in each band were corrected for the Galactic dust extinction and for the internal dust extinction in galaxies. The values for Galactic extinctions in different bands are taken from Schlegel et al (1998). The high Galactic latitude ($\sim -52^\circ$) of the Eridanus group results in minimal Galactic extinction. The average values of the Galactic extinctions toward Eridanus are 0.112 mag in the R-band, 0.037 mag in the J-band, 0.024 mag in the H-band, and 0.015 mag in the K-band. The estimation of internal dust extinction in galaxies is quite uncertain. Several authors have discussed the methods to correct the magnitudes for the internal extinction (e.g., Tully & Fouque 1985, Tully et al. 1998, Masters et al. 2003) have discussed internal extinction in galaxies. The prescription of Tully & Fouque (1985) is based on an assumption where some fraction ($\sim$ 0.1) of stars are mixed with dust whose opacity is wave-band dependent. The main caveat in this prescription is that it does not take take into account either the total luminosity or the Hubble type of the galaxy. However, it is natural to believe that more luminous galaxies will have more dust. The dust content will also be type dependent as it is known that early type galaxies (E+S0) do not have much cold interstellar matter in them. Tully et al. (1998) and Masters et al. (2003) obtained empirically a relation between the total luminosity and the dust content in late type disk galaxies. The extinction, A_λ^i, is given as a function of the axial ratio (b/a) in the pass-band λ as:

$$A_\lambda^i = \gamma_\lambda\ log\ (a/b) \tag{4.4}$$

Where a is the length of the semi-major axis and b is the length of the semi-minor axis. The γ were estimated in each band using the following relations.

R-band:

if $M_R > -16.2$ mag:

$$\gamma_R = 0 \tag{4.5}$$

if $M_R < -16.2$ mag:

$$\gamma_R = -0.24(16.2 + M_R) \tag{4.6}$$

J-band:
if $M_J > -22.2$ mag:

$$\gamma_J = -0.26(M_J + 23) + 0.77 \tag{4.7}$$

if $M_J < -22.2$ mag:

$$\gamma_J = -0.04(M_J + 23) + 0.60 \tag{4.8}$$

H-band:
if $M_H > -22.2$ mag:

$$\gamma_H = -0.26(M_H + 23) + 0.58 \tag{4.9}$$

if $M_H < -22.2$ mag:

$$\gamma_H = -0.01(M_H + 23) + 0.38 \tag{4.10}$$

K-band:
if $M_K > -22.2$ mag:

$$\gamma_K = -0.13(M_K + 23) + 0.31 \tag{4.11}$$

if $M_K < -22.2$ mag:

$$\gamma_K = 0.20 \tag{4.12}$$

The dust opacity has a subtle and important effect on the exponential surface brightness of disks. If galaxies were completely transparent, then, the central disk surface brightness $\mu_0(\lambda)$ is expected to become brighter with increasing inclination. On the other hand, for a finite optical depth of disks, the following expression will result:

$$\mu_0^{b,i}(\lambda) = \mu_0(\lambda) - 2.5C_\lambda log(b/a) \tag{4.13}$$

where $\mu_0^{b,i}(\lambda)$ is the face-on (corrected) value of the central disk surface brightness, b/a is the minor to major axis ratio of the inclined disk, C_λ is a constant, the value of which is between 0 (opaque) and 1 (transparent), and, depends on the wave-band. Following Tully & Verheijen (1997), the value for C_λ is 0.52 for the R band. In the near-IR bands, C_λ is taken as 1 (cf. Graham 2001).

4.5 $\mu_0^i - logr_d$ relation and HSB–LSB dichotomy

The well known Freeman's law for disk galaxies that the central disk surface brightness of spiral galaxies is constant at $\mu_0^B = 21.65 \pm 0.30$ mag arcsec^{-2} (cf. Freeman 1970) has been understood as due to high degree of opacity of spiral disks in the optical bands (see e.g., Davies & Burstein 1995). The current view is that the central disk surface brightnesses of galaxies are distributed over a large range spanning more than 5 magnitudes (McGaugh et al. 1995, McGaugh 1996, de Jong 1996, Tully & Verheijen 1997). Tully & Verheijen (1997) reported that the average central disk surface brightness of high surface brightness (HSB) galaxies differs by at least two magnitudes than that of the low surface brightness (LSB) galaxies in both the optical and the near-infrared bands. This indicates a possible bimodal nature of the central disk surface brightnesses.

It is noticed that in the Eridanus group, the central surface brightness of disks are correlated with the morphological types and disk scale lengths. Fig. 4.2 shows that galaxies with H.T. > 6 have fainter central surface brightness than the galaxies of earlier types in all bands. There is also a hint in Fig. 4.2 that μ_0^i increases linearly with increasing Hubble type. The difference in μ_0^i is at least 1 mag between galaxies later and earlier than Sc (H.T. = 6). It confirms the results of van der kruit (1987) that the fainter late-type galaxies ($>$ Sc) do not follow Freeman's law made with the earlier type ($<$ Sc) disk galaxies.

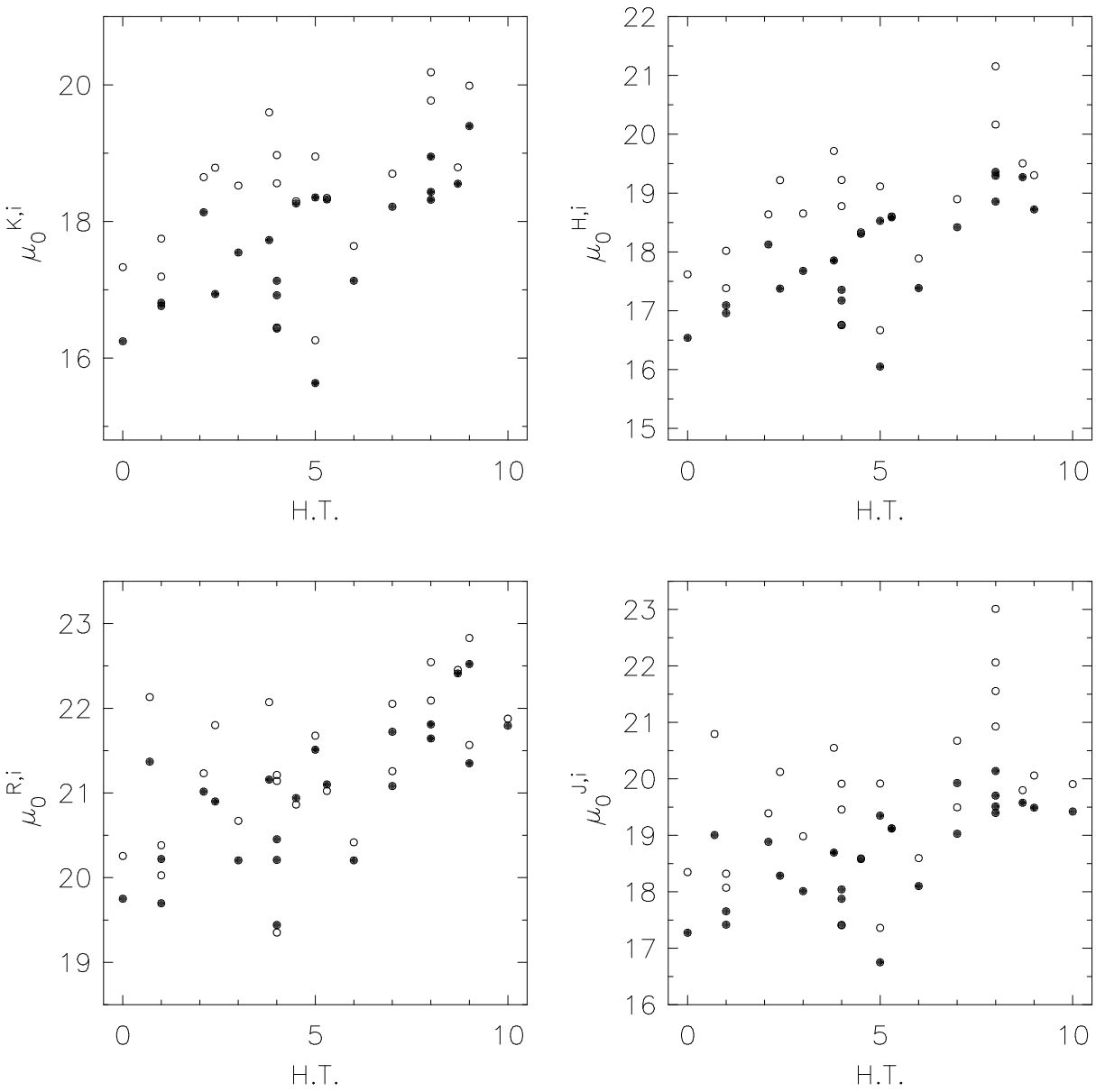

Figure 4.2: The central disk surface brightness (in ordinate) plotted against the Hubble type (in abscissa). The open symbols are inclination corrected and filled symbols are uncorrected values of the surface brightness. A morphological dependence is clearly seen in this plot.

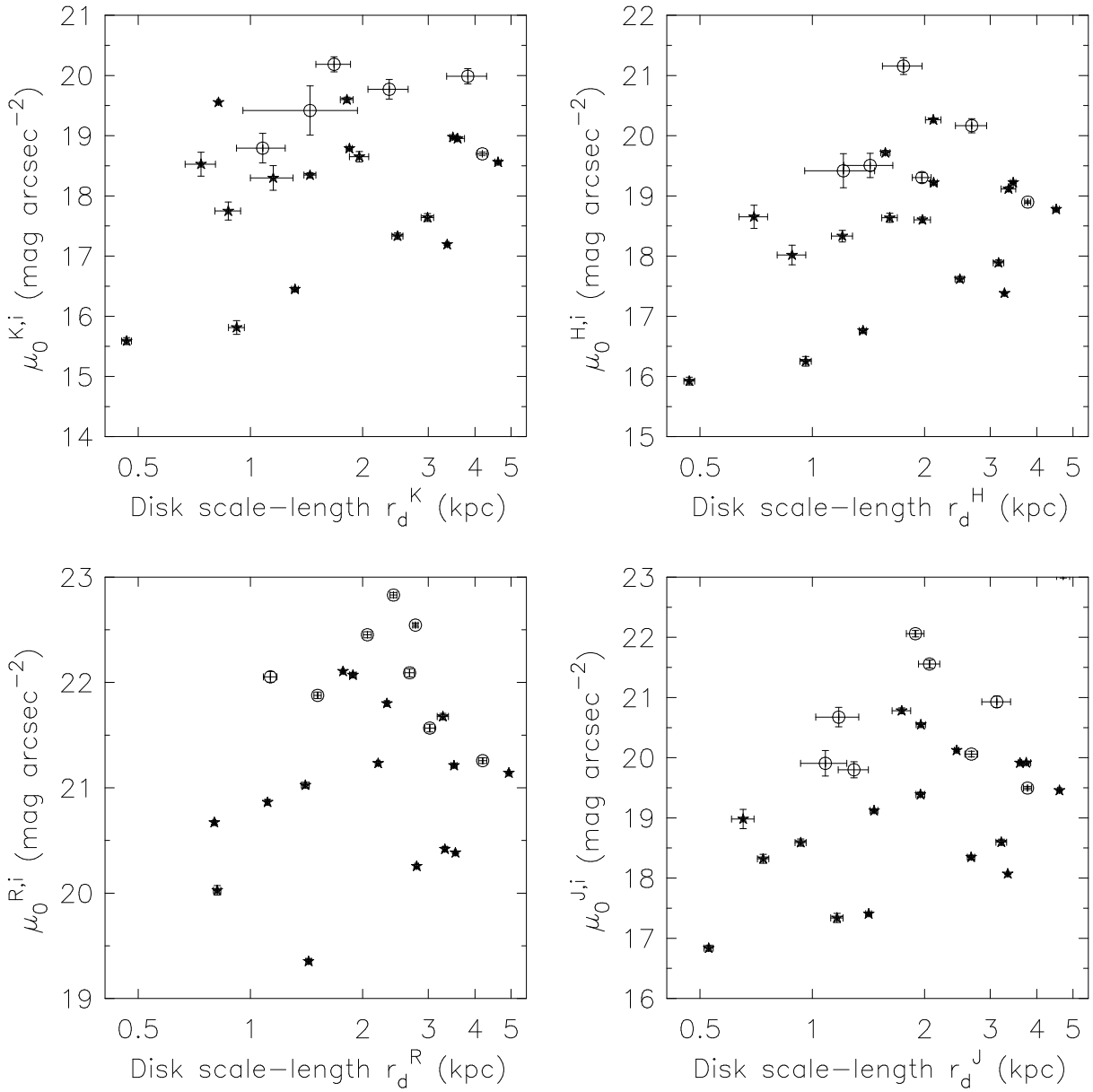

Figure 4.3: The central disk surface brightness in different bands is plotted against the scale lengths in their respective bands. The open symbols are galaxies later than Hubble type 6, and filled symbols are galaxies earlier than Hubble type 6. In the K-band, there appears to be a linear correlation between $\mu_0 - logr_d$ for HSB's ($15 < \mu_0^K < 19$ mag arcsec^{-2}) and LSB's ($18 < \mu_0^K < 20$ mag arcsec^{-2}) separately.

Graham (2001) reported that in the K-band, for the early type (< Sc) disk galaxies, μ_0 increases with increasing disk scale length (r_d) such that $\mu_0 \propto 2logr_d$. The inclination corrected central disk surface brightness μ_0^i is plotted against the disk scale length in Fig. 4.3 where a similar trend as reported by Graham (2001) can be seen where μ_0^i increases linearly with logr_d. This effect is more prominent in the K band than in other bands, probably due to minimal effects of dust extinction in the K-band. In fact, there is a hint of bi-modality in this plot in the sense that galaxies occupy two regions in the $\mu_0 - logr_d$ relation with LSB's in the range $18 < \mu_0^K < 20$ mag arcsec^{-2}, and HSB's in the range $15 < \mu_0^K < 19$ mag arcsec^{-2}, and, both HSB's and LSBs following $\mu_0 - logr_d$ relation with same slope. This result and other similar results (e.g., Tully & Verheijen 1997, Graham 2001) suggests that HSB's and LSB's occupy two different parameter space in their disk properties.

4.6 Results

An optical atlas is prepared for galaxies observed in the R band and some other galaxies for which no R band observations were made, but, were detected in H I described in chapter 3. The photometric properties and structural parameters of galaxies are presented in a tabular form. The description of the atlas and the table are as follows:

Atlas The layout of the atlas is shown in Fig. 4.4. The R band image is shown in the upper left hand corner, and J band image is shown in the upper right hand corner of the atlas. The gray scale levels are adjusted so that high surface brightness regions and low surface brightness regions can be distinguished. A bar of length 5 kpc is shown at the top right hand corner of both the images. In the left lower half of the atlas, surface brightness profiles in the R, J, and K bands are shown in different symbols. The (R-J) color profile is shown below this panel. On the right hand side of the lower half of the atlas, the R band surface brightness profile is shown separately for receding and approaching half of the galaxy. The aim of this plot is to look for lopsidedness in galaxies. Below this plot, the total magnitudes in the R, J, H, and K bands, R band scale length, and R band central disk surface brightness corrected for inclination are written. All profiles are corrected for the Galactic extinction.

Table The results obtained from the above analyses of the optical and near-IR images are presented in Tab. 4.2. The description of the entries in each column of this table is as follows :

Column 1 : The name of the galaxy in tan abbreviated format. The ESO galaxies are written as E, NGC is written as N, UGCA is written as U, IC is written as I, MCG is written as M, and SGC is written as S.

Column 2 : The morphological type, position angle and inclination with associated errors in the estimation determined from the R band observations or from DSS images when R band observations were not available, radius in kpc at 25 mag arcsec^{-2} B band isophote taken from RC3. The P.A. is measured from North to East (counter-clockwise).

Column 3 : The filter (band) used.

Column 4&5 : The disk scale length and associated errors in the fitting procedure in units of kpc.

Column 6 : The radius in kpc corresponding to the isophotal level of 25 mag arcsec^{-2} in the R, 21 mag arcsec^{-2} in the J, 20.5 mag arcsec^{-2} in the H, and 20 mag arcsec^{-2} in the K band.

Column 7, 8, &9 : The central surface brightness of the disk as obtained from the fit, and the values corrected for the inclination, Galactic extinction, and internal extinction. The error is obtained from the fitting procedure and does not include calibration errors.

Column 10 : The isophotal magnitude of the galaxy estimated within the fixed aperture at 26.0 mag arcsec^{-2} for the R-band, 21.0 mag arcsec^{-2} in the J band, 20.5 mag arcsec^{-2} in the H band, and 20.0 mag arcsec^{-2} in the K band.

Column 11 :The total magnitude extrapolated to infinity with corrections for Galactic and internal extinctions.

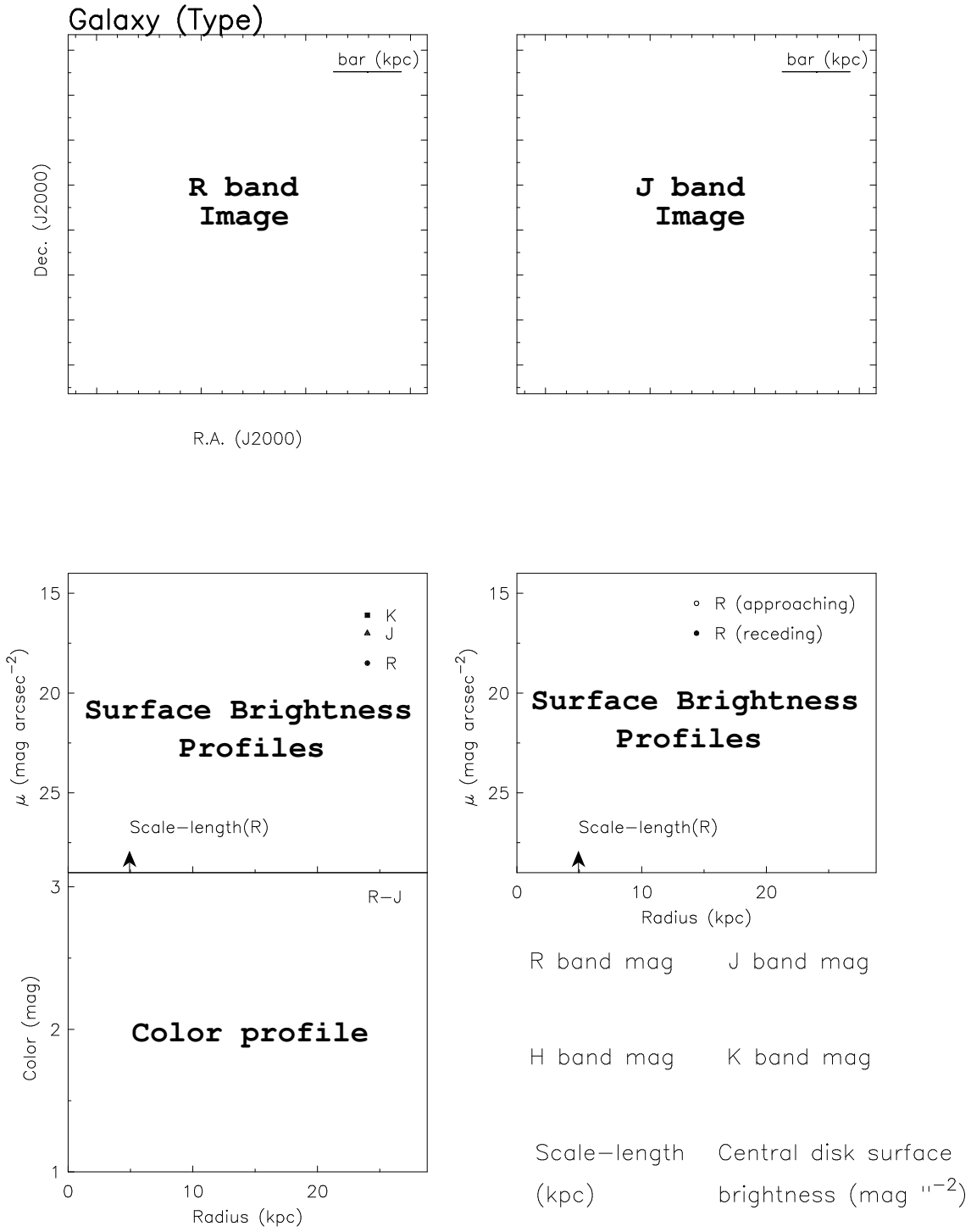

Figure 4.4: The layout of the optical atlas

Table 4.2: Photometric Results

Galaxy	Type P.A.± Incl.± r(B_{25}) (kpc)	F	r_d ±	$r_{(25)}$ $r_{(21)}$ $r_{(20.5)}$ $r_{(20)}$ (kpc)	μ^0	$\mu^{0,i}$ ±	m_{26} m_{21} $m_{20.5}$ m_{20} (mag)	m^{total}
			(kpc)		(mag arcsec^{-2})			(mag)
E 482-005	SBdm	R	–	–		–	–	
	79 0	J	1.89 0.10	2.5	19.51	22.06 0.05	15.10	14.50
	85 2	H	–	–		–	–	–
	5.6	K	–	–		–	–	–
E 482-013	Sb	R	0.80 0.01	3.6	20.20	20.67 0.02	14.97	14.80
	57 1	J	0.65 0.05	1.8	18.01	18.98 0.16	13.66	13.51
	66 3	H	0.70 0.06	1.8	17.68	18.65 0.19	13.17	13.02
	3.8	K	0.74 0.07	1.6	17.55	18.53 0.20	13.04	12.62
E 482-035	SBab	R	2.20 0.03	7.4	21.02	21.23 0.02	13.19	12.94
	4 1	J	1.95 0.05	3.6	18.89	19.39 0.04	11.76	11.18
	52 1	H	1.61 0.08	3.6	18.13	18.64 0.08	11.18	10.72
	4.4	K	1.96 0.12	3.4	18.14	18.65 0.09	11.03	10.35
E 548-021	SBdm	R	–	–		–	–	–
	70 1	J	4.71 0.20	5.6	19.40	23.01 0.02	14.12	13.33
	88 0	H	3.37 0.23	4.5	18.86	22.48 0.05	14.15	13.62
	6.7	K	3.71 0.34	4.5	18.43	22.06 0.06	13.68	12.81
E 548-036	S?	R	–	–		–	–	–
	170 2	J	0.65 0.01	2.5	16.75	17.36 0.04	11.56	11.40
	56 2	H	0.61 0.02	2.5	16.05	16.67 0.06	10.88	10.76
	3.4	K	0.59 0.01	2.2	15.64	16.26 0.07	10.58	10.45
E 548-49	S?	R	1.13 0.05	3.1	21.72	22.05 0.05	15.69	15.49
	112 1	J	1.18 0.16	1.1	19.93	20.67 0.16	15.35	14.20
	61 2	H	–	–		–	–	–
	3.4	K	–	–		–	–	–
E 548-065	SBa	R	1.77 0.01	5.8	21.34	22.11 0.01	15.31	14.85
	41 0	J	1.74 0.10	2.2	18.99	20.78 0.05	13.98	13.51
	80 1	H	–	–		–	–	–
	5.0	K	–	–		–	–	–
E 549-002	IBm	R	1.51 0.03	4.5	21.79	21.88 0.03	14.73	14.34
	32 1	J	1.08 0.15	1.3	19.42	19.91 0.21	14.28	13.48
	53 1	H	–	–		–	–	–
	4.4	K	–	–		–	–	–

E 549-18	SABc	R	3.28	0.11	8.7	21.51	21.68	0.03	12.91	12.51
	23 1	J	3.75	0.11	6.0	19.35	19.92	0.03	11.07	10.15
	56 1	H	3.36	0.15	6.0	18.53	19.11	0.04	10.39	9.69
	5.0	K	3.59	0.16	5.8	18.35	18.95	0.04	10.25	9.34
I 1952	SBbc	R	3.52	0.06	11.2	20.21	21.21	0.02	13.05	12.42
	140 0	J	3.60	0.04	9.0	17.88	19.91	0.01	10.78	10.26
	81 0	H	3.46	0.06	9.0	17.17	19.22	0.02	10.15	9.72
	8.7	K	3.49	0.07	7.8	16.92	18.97	0.02	9.98	9.62
I 1953	SBd	R	4.20	0.11	12.1	21.08	21.26	0.03	11.95	11.62
	121 0	J	3.78	0.10	7.4	19.03	19.50	0.03	10.39	9.68
	51 1	H	3.78	0.07	7.6	18.42	18.90	0.02	9.75	9.13
	9.4	K	4.19	0.13	7.2	18.22	18.70	0.03	9.51	8.77
I 1962	SBdm	R	2.77	0.05	9.2	21.64	22.54	0.02	14.62	14.16
	1 1	J	2.06	0.14	2.5	19.70	21.56	0.07	14.45	13.57
	80 2	H	1.76	0.21	2.0	19.29	21.16	0.14	14.44	13.60
	9.1	K	1.68	0.18	2.7	18.32	20.19	0.13	13.19	12.40
M-03-10-041	SBdm	R	2.67	0.08	6.9	21.81	22.09	0.04	13.99	13.56
	166 1	J	3.13	0.28	2.0	20.14	20.93	0.10	13.54	11.89
	63 1	H	2.68	0.26	2.7	19.36	20.17	0.12	12.59	11.37
	6.7	K	2.36	0.29	2.0	18.95	19.77	0.16	12.63	11.26
N 1309	SAbc	R	1.43	0.02	6.7	19.44	19.35	0.03	11.91	11.78
	25 0	J	1.42	0.03	4.5	17.41	17.41	0.03	10.05	9.84
	14 4	H	1.37	0.03	4.3	16.75	16.76	0.03	9.46	9.29
	7.4	K	1.32	0.03	4.3	16.43	16.45	0.03	9.22	9.04
N 1325	SAbc	R	4.93	0.03	19.3	20.45	21.14	0.01	11.75	11.12
	53 1	J	4.60	0.06	11.7	18.04	19.46	0.01	9.74	9.17
	75 0	H	4.51	0.09	12.3	17.36	18.78	0.03	9.06	8.63
	15.8	K	4.61	0.09	10.8	17.13	18.56	0.02	8.88	8.48
N 1345	SBc	R	1.11	0.01	4.3	20.94	20.86	0.03	13.74	13.58
	90 0	J	0.93	0.03	2.0	18.58	18.59	0.06	12.20	11.76
	17 12	H	1.20	0.08	2.2	18.31	18.33	0.10	11.49	10.97
	5.0	K	1.15	0.15	1.3	18.27	18.30	0.20	11.70	10.97
N 1347	SBcd	R	1.40	0.03	4.3	21.10	21.03	0.03	13.79	13.63
	120 0	J	1.46	0.03	2.2	19.12	19.12	0.03	12.44	11.78
	14 3	H	1.97	0.10	3.6	18.59	18.60	0.05	11.07	10.43
	3.5	K	1.44	0.05	2.5	18.32	18.34	0.04	11.52	10.76

N 1359	SBcm	R	3.03	0.09	9.0	21.35	21.57	0.04	12.83	12.48
	325 0	J	2.67	0.10	4.0	19.49	20.06	0.05	11.95	11.00
	55 0	H	–		3.6	18.72	19.30	0.08	11.57	10.85
	8.1	K	–		1.6	19.40	19.99	0.13	12.34	10.16
N 1371	SABa	R	3.55	0.02	17.2	20.22	20.38	0.01	10.98	10.69
	134 1	J	3.34	0.02	10.3	17.65	18.07	0.01	8.75	8.42
	48 1	H	3.28	0.02	10.8	16.96	17.38	0.01	8.06	7.81
	18.8	K	3.37	0.04	9.6	16.76	17.19	0.01	7.87	7.60
N 1385	SBcd	R	3.32	0.04	15.2	20.20	20.42	0.02	11.14	10.84
	173 1	J	3.21	0.10	8.7	18.10	18.60	0.05	9.43	9.02
	51 1	H	3.16	0.10	9.2	17.39	17.89	0.05	8.72	8.40
	11.4	K	2.98	0.11	8.1	17.13	17.64	0.07	8.60	8.26
N 1390	SB0/a	R	0.81	0.02	4.5	19.70	20.03	0.04	14.33	13.98
	23 1	J	0.74	0.03	2.5	17.42	18.32	0.07	12.54	12.36
	66 1	H	0.88	0.08	2.5	17.09	18.02	0.16	11.84	11.66
	4.7	K	0.87	0.07	2.2	16.81	17.75	0.15	11.69	11.41
N 1414	SBbc	R	1.88	0.04	5.6	21.16	22.07	0.02	15.18	14.86
	170 1	J	1.96	0.06	3.8	18.69	20.55	0.03	12.95	12.54
	80 1	H	1.57	0.04	4.0	17.85	19.72	0.04	12.37	12.13
	5.8	K	1.81	0.07	3.4	17.73	19.60	0.04	12.23	11.71
N 1415	SAB0/a	R	2.79	0.03	16.4	19.75	20.26	0.02	11.56	11.04
	151 1	J	2.67	0.06	8.5	17.28	18.35	0.03	9.39	8.99
	69 1	H	2.49	0.07	8.1	16.54	17.62	0.04	8.73	8.44
	11.8	K	2.48	0.08	7.8	16.25	17.33	0.05	8.42	8.17
N 1422	SBab	R	2.32	0.03	9.2	20.90	21.80	0.02	14.30	13.86
	66 0	J	2.44	0.03	5.8	18.29	20.12	0.01	11.87	11.43
	80 1	H	2.12	0.05	5.8	17.38	19.22	0.03	11.15	10.85
	7.4	K	1.84	0.03	5.4	16.94	18.79	0.02	10.98	10.65
N 1481	SA0	R	–		–		–		–	–
	129 6	J	0.60	0.07	1.8	17.88	18.21	0.22	12.57	12.32
	45 1	H	0.63	0.03	1.8	17.24	17.60	0.09	11.86	11.64
	3.4	K	0.72	0.03	1.8	17.09	17.45	0.08	11.55	11.24
N 1482	SA0/a	R	–		–		–		–	–
	105 1	J	1.17	0.04	5.4	16.66	17.34	0.08	9.84	9.57
	59 2	H	0.96	0.03	4.9	15.57	16.25	0.08	9.03	8.85
	8.4	K	0.92	0.04	4.9	15.12	15.81	0.11	8.57	8.44

S 0321.2-1929	IBm	R	2.10	0.20	0.2	24.79	24.83	0.065	17.99	16.76
	170 0	J	–		–		–		–	–
	36 6	H	–		–		–		–	–
	4.4	K	–		–		–		–	–
U 068	SABcdm	R	2.06	0.05	5.2	22.41	22.45	0.03	14.53	14.24
	42 1	J	1.29	0.12	1.3	19.58	19.80	0.13	13.84	12.90
	38 3	H	1.43	0.22	1.3	19.27	19.51	0.20	13.75	12.66
	5.7	K	1.08	0.16	1.3	18.55	18.79	0.24	13.08	12.15
U 077	SBdm	R	2.42	0.05	6.0	22.52	22.83	0.02	14.97	14.51
	138 1	J	–		–		–		–	–
	64 1	H	–		–		–		–	–
	5.7	K	–		–		–		–	–

Bibliography

[1] Bell, E. F. & de Jong R.S. 2001, *ApJ*, **550**, 212

[2] Davies, J. I., & Burstein, D. 1995, *Proceedings of the NATO advanced study institute, ed. by Davies, J.I. & Burstein, D.*, (Kluwer Academic Publishers)

[3] de Jong, R. S. 1996, *AA Supl.*, **118**, 557

[4] Freeman, K.C 1970, *ApJ*, **160**, 811

[5] Graham, A. W. 2001, *MNRAS*, **326**, 543

[6] Hubble, E. P 1926, *ApJ*, **64**, 321

[7] Jarret, T. H., Chester, T., Cutri, R., Schneider, S., Skrutskie, M., & Huchra, J. P. 2000, *AJ*, **119**, 2498

[8] Landolt, A.U. 1992, *AJ*, **104**, 340

[9] McGaugh, S. S., Bothun, G. D., & Schombert, J. M. 1995, *AJ*, **110**, 573

[10] McGaugh, S. S. 1996, *MNRAS*, **280**, 337

[11] Schlegel, D. J., Finkbeiner, D. P., & Davis, M. 1998, *ApJ*, **500**, 525

[12] Tully, R. B., Verheijen, M. A. W., Pierce, M. J., Huang, J., & Wainscoat, R. J. 1996, *AJ*, **112**, 2471

[13] Tully, R. B., & Verheijen, M. A. W. 1997, *ApJ*, **484**, 145

[14] Tully, R. B., & Fouque, P. 1985, *ApJ Supl.*, **58**, 67

[15] Tully, R. B., Pierce, M. J., Huang, J., Saunders, W., Verheijen, M. A. W., & Witchalls, P. L. 1998, *AJ*, **115**, 2264

[16] van der Kruit, P. C. 1987, *A&A*, **173**, 59

The Optical Atlas

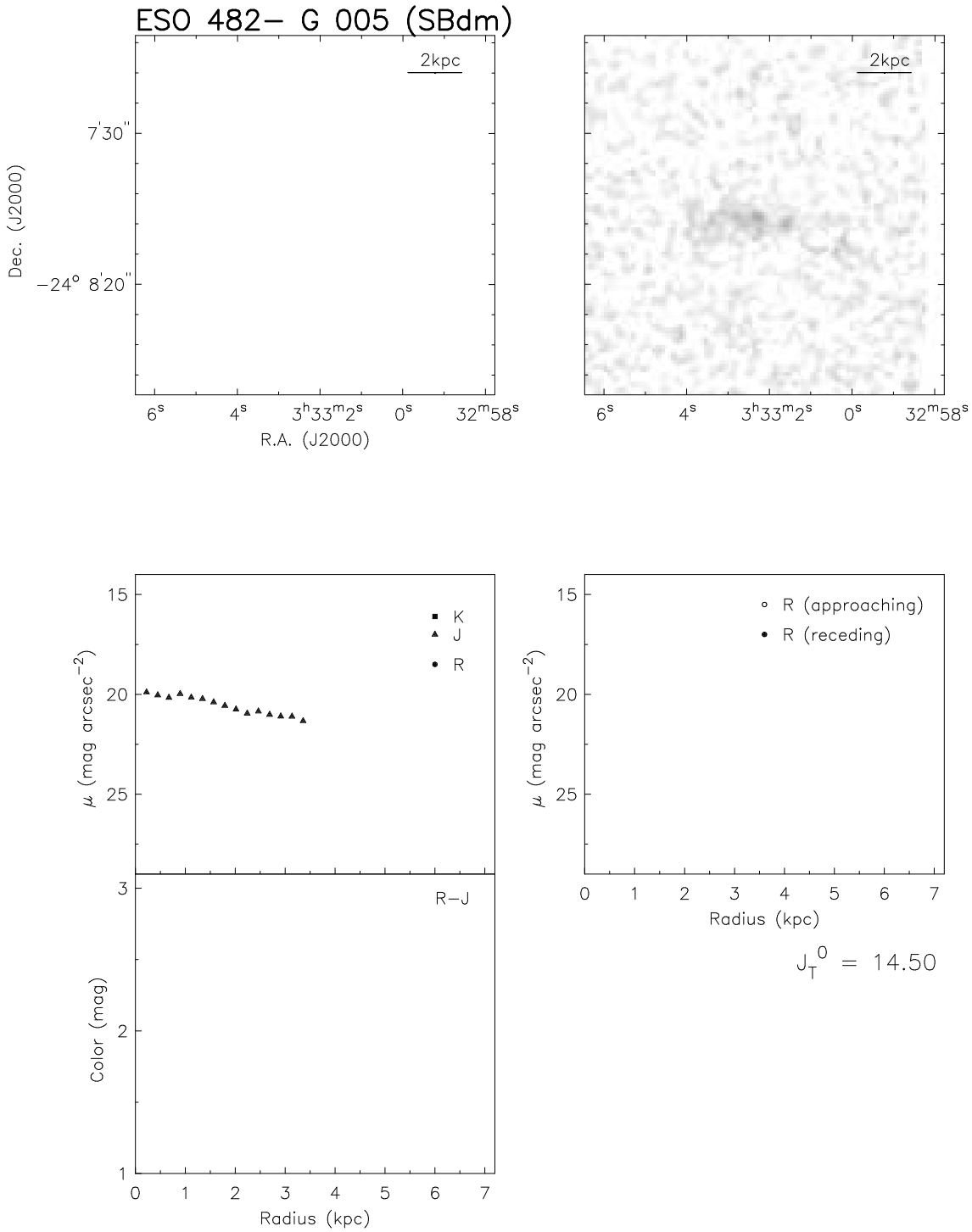
ESO 482− G 005 (SBdm)
2kpc
7'30"
−24° 8'20"
Dec. (J2000)
6s
4s
3h33m2s
0s
32m58s
R.A. (J2000)
2kpc
6s
4s
3h33m2s
0s
32m58s
15
20
25
μ (mag arcsec−2)
K
J
R
R−J
3
2
1
Color (mag)
0 1 2 3 4 5 6 7
Radius (kpc)
15
20
25
μ (mag arcsec−2)
R (approaching)
R (receding)
0 1 2 3 4 5 6 7
Radius (kpc)
J_T^0 = 14.50

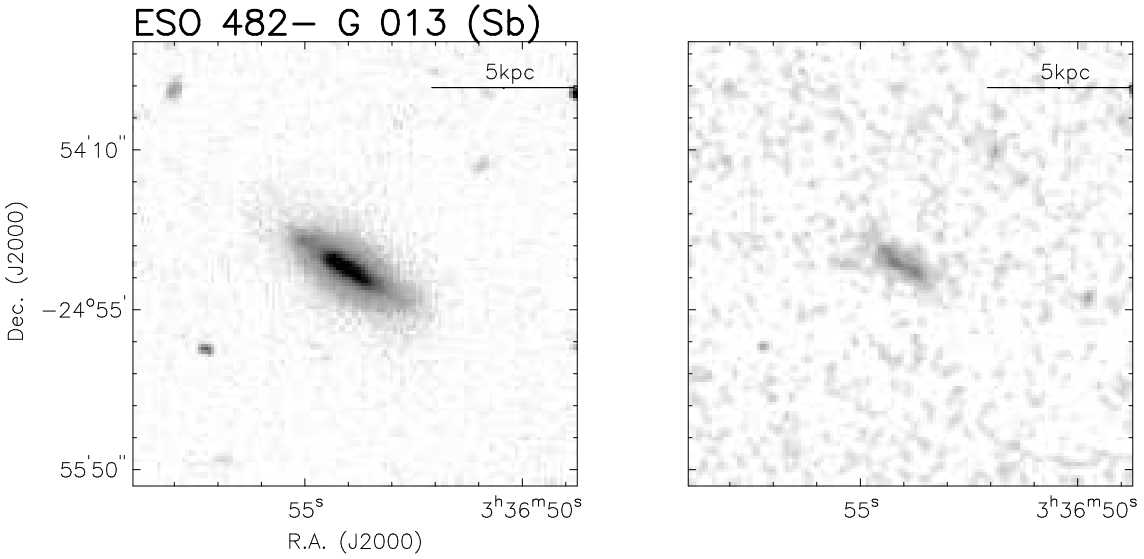

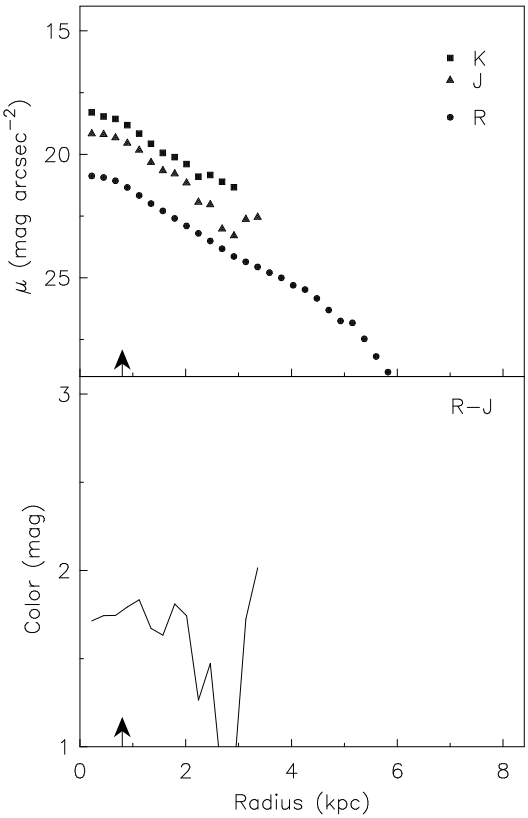

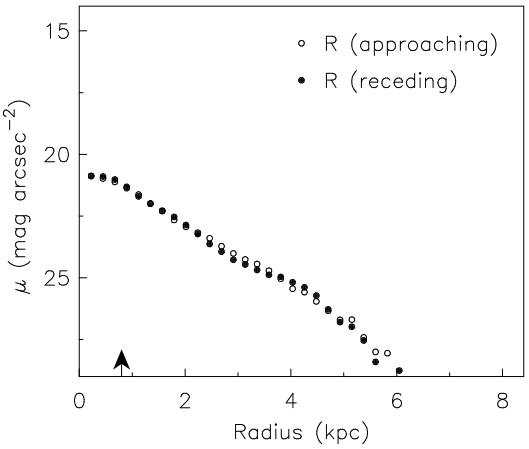

$R_T^0 = 14.79$ $J_T^0 = 13.51$

$H_T^0 = 13.02$ $K_T^0 = 12.62$

$r_d^R = 0.8$ $\mu_R^{0,i} = 20.67$

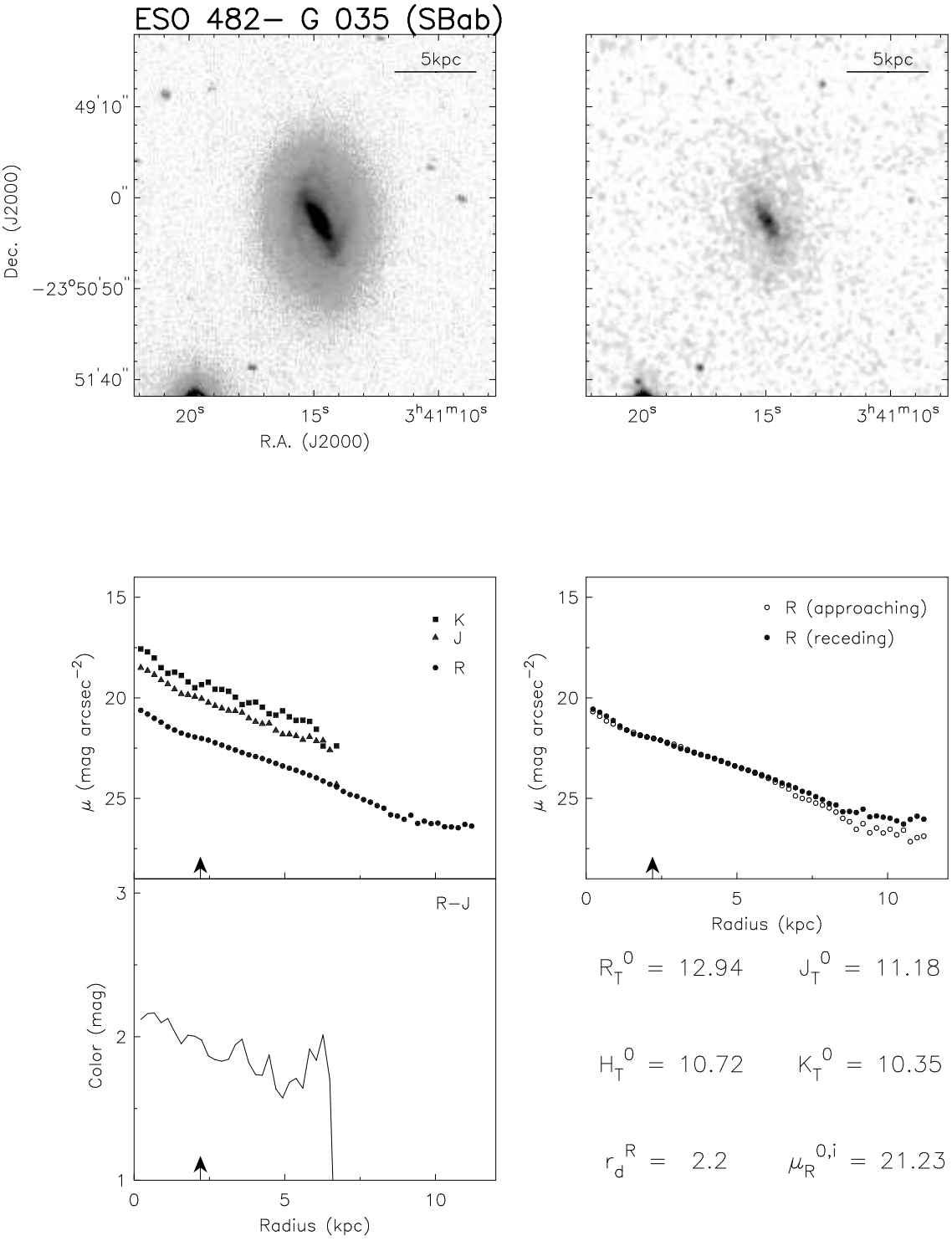
ESO 482− G 035 (SBab)
5kpc
5kpc
Dec. (J2000)
49'10"
0"
−23°50'50"
51'40"
20s
15s
3h41m10s
R.A. (J2000)
μ (mag arcsec−2)
K
J
R
R−J
Color (mag)
Radius (kpc)
R (approaching)
R (receding)
R_T^0 = 12.94
J_T^0 = 11.18
H_T^0 = 10.72
K_T^0 = 10.35
r_d^R = 2.2
$\mu_R^{0,i}$ = 21.23

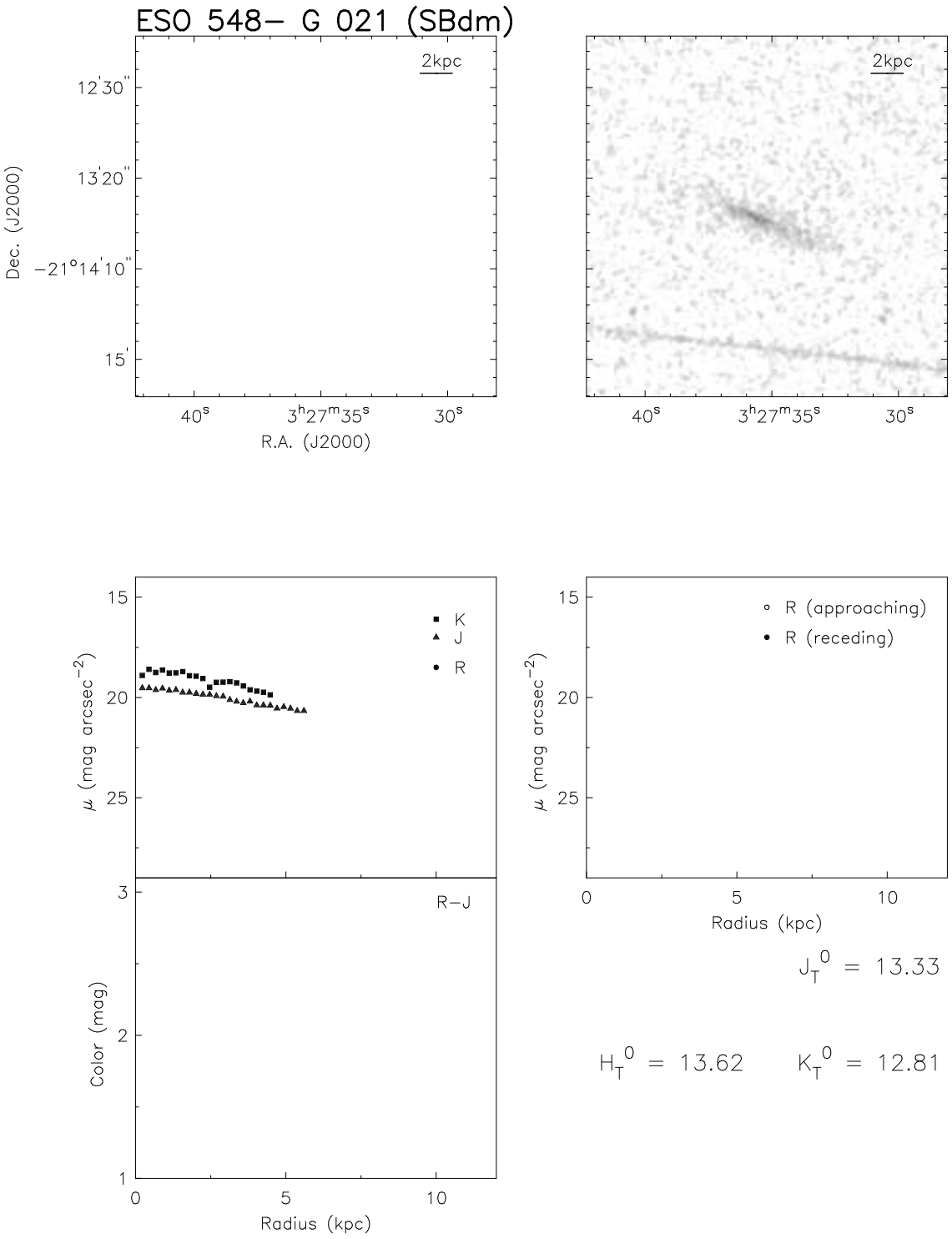

$J_T^0 = 13.33$

$H_T^0 = 13.62$ $K_T^0 = 12.81$

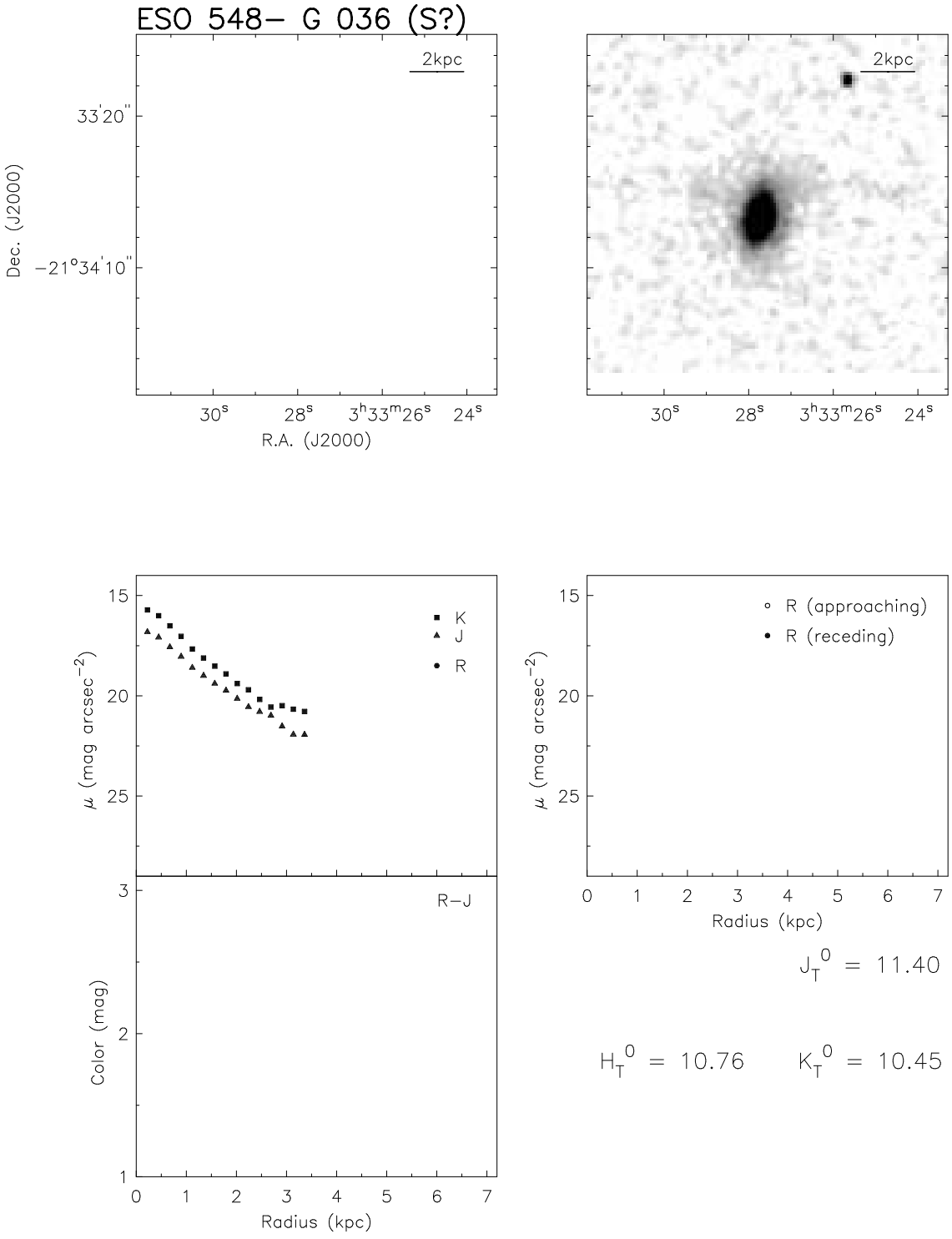

$J_T^0 = 11.40$

$H_T^0 = 10.76$ $K_T^0 = 10.45$

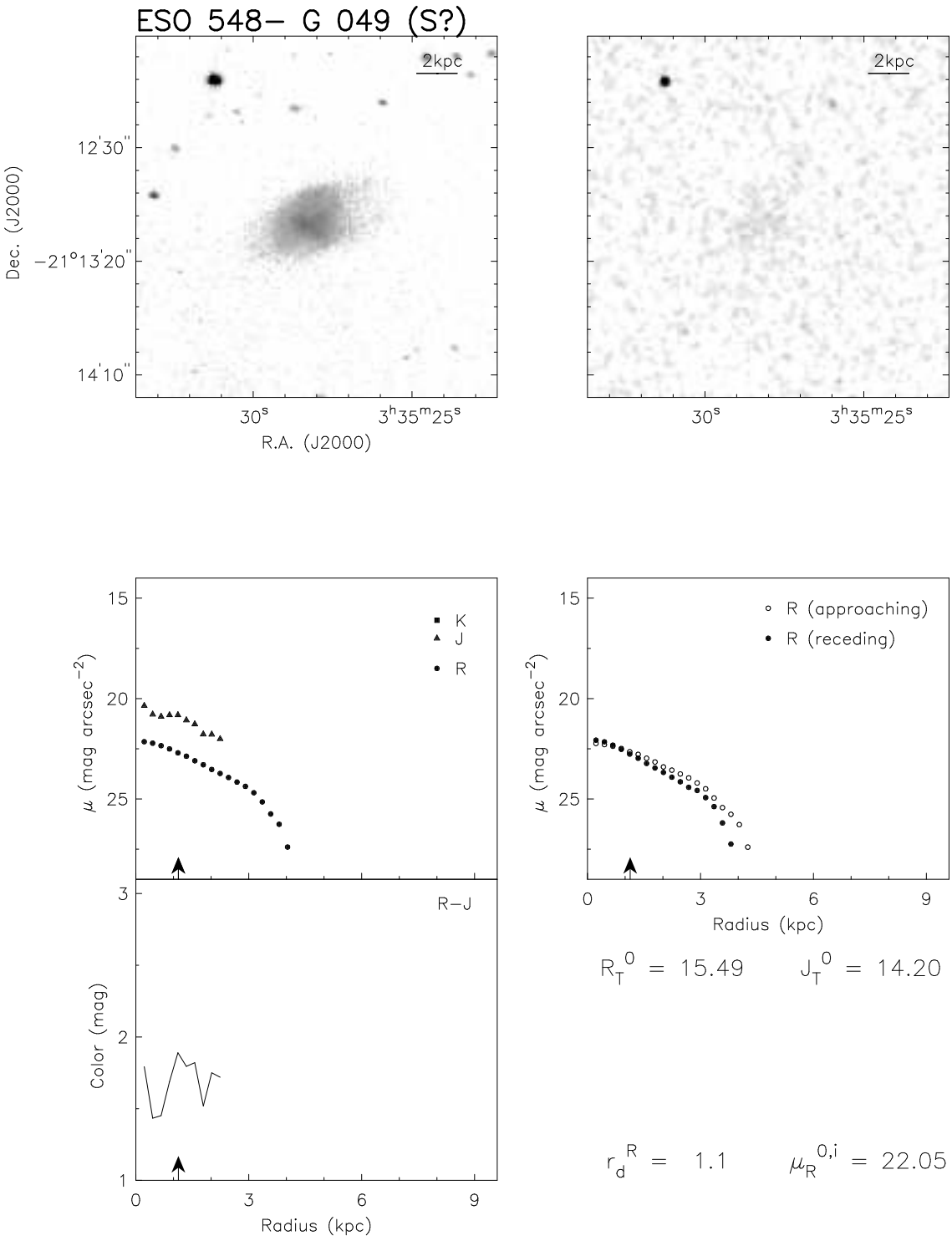
ESO 548– G 049 (S?)
2kpc
12'30"
−21°13'20"
14'10"
Dec. (J2000)
30s
3h35m25s
R.A. (J2000)
2kpc
30s
3h35m25s
K
J
R
μ (mag arcsec−2)
15
20
25
R−J
Color (mag)
3
2
1
0
3
6
9
Radius (kpc)
R (approaching)
R (receding)
μ (mag arcsec−2)
15
20
25
0
3
6
9
Radius (kpc)
R_T^0 = 15.49
J_T^0 = 14.20
r_d^R = 1.1
μ_R^0,i = 22.05

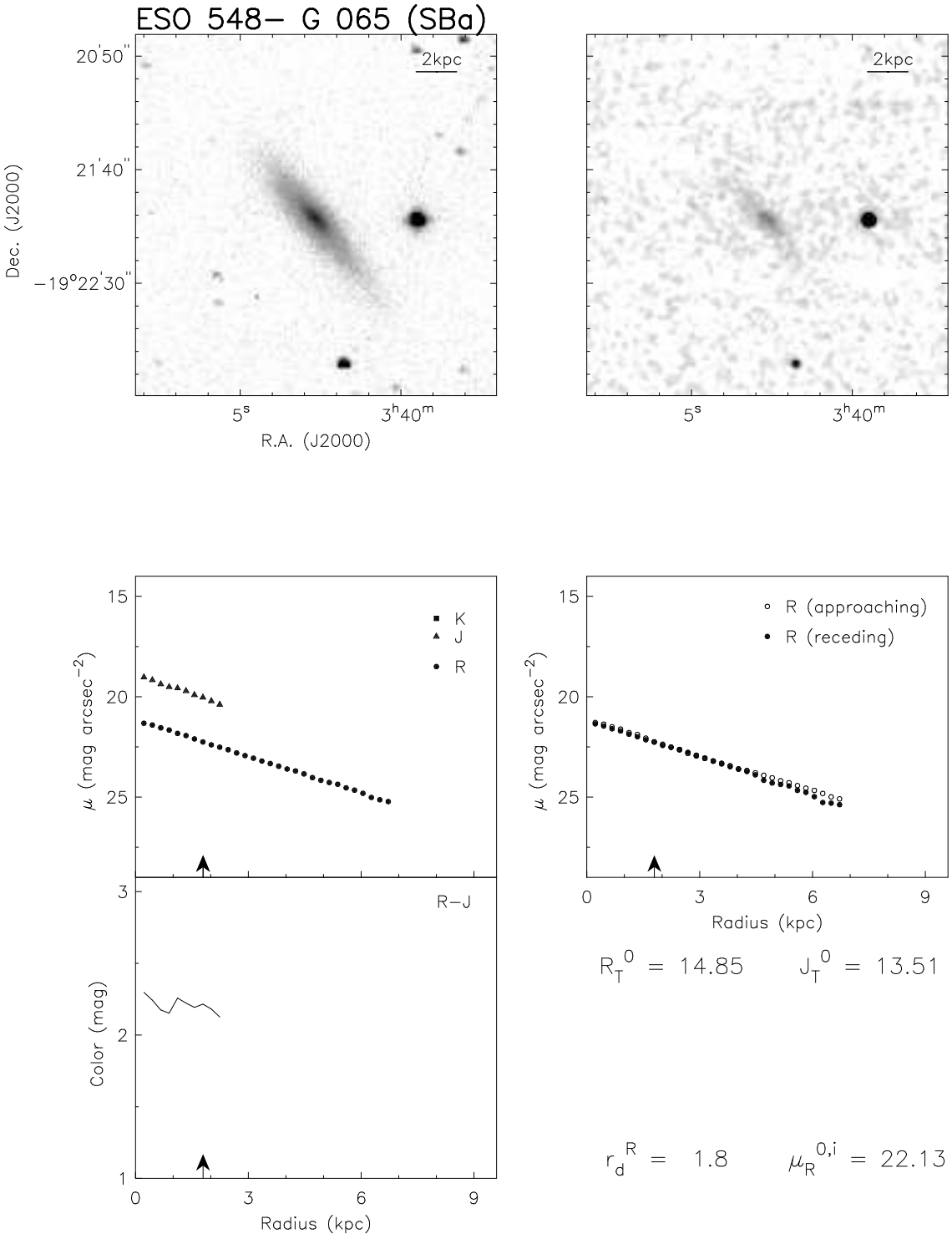

$R_T^0 = 14.85$ $J_T^0 = 13.51$

$r_d^R = 1.8$ $\mu_R^{0,i} = 22.13$

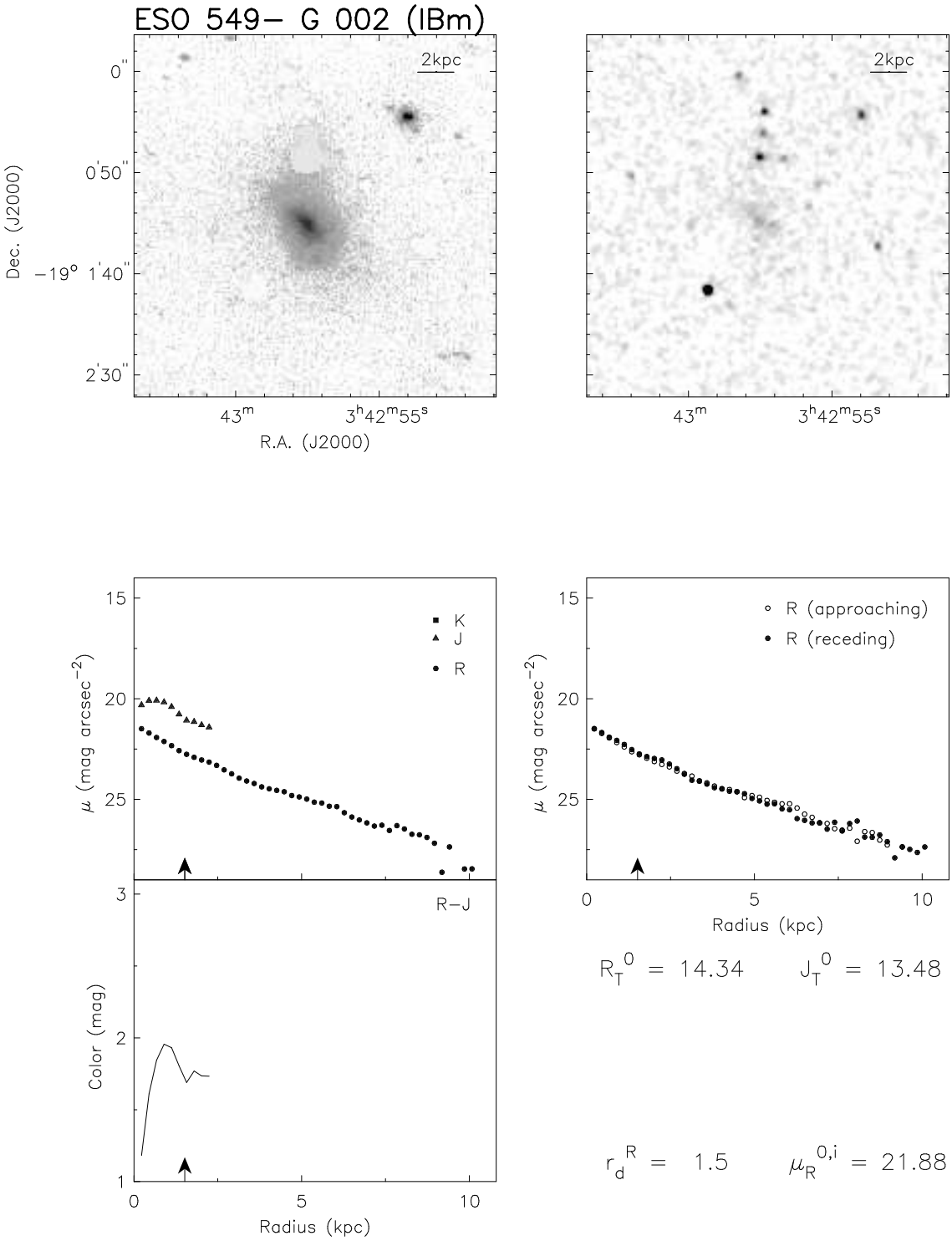

$R_T^0 = 14.34$ $J_T^0 = 13.48$

$r_d^R = 1.5$ $\mu_R^{0,i} = 21.88$

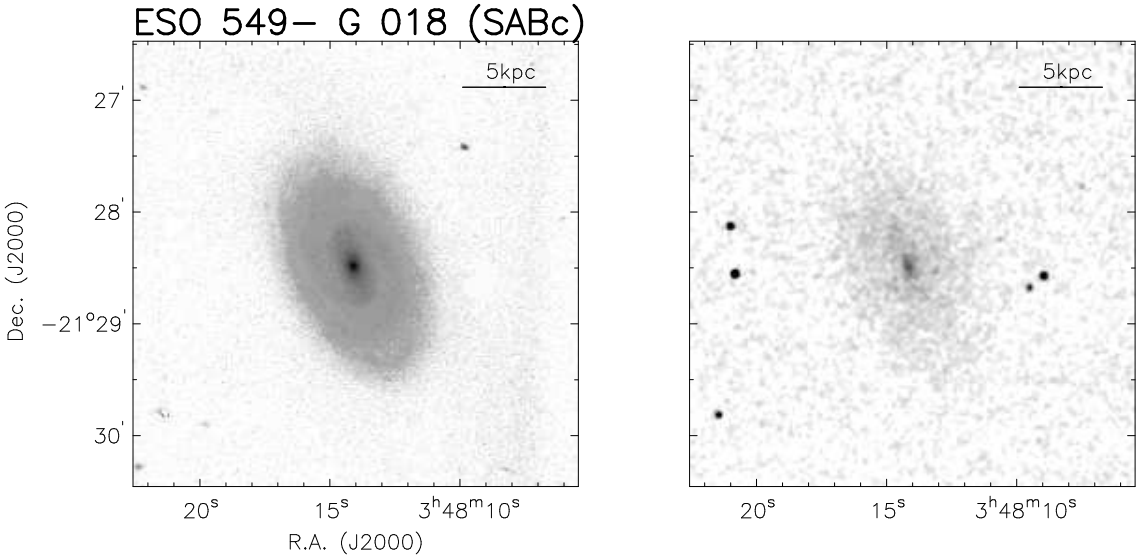

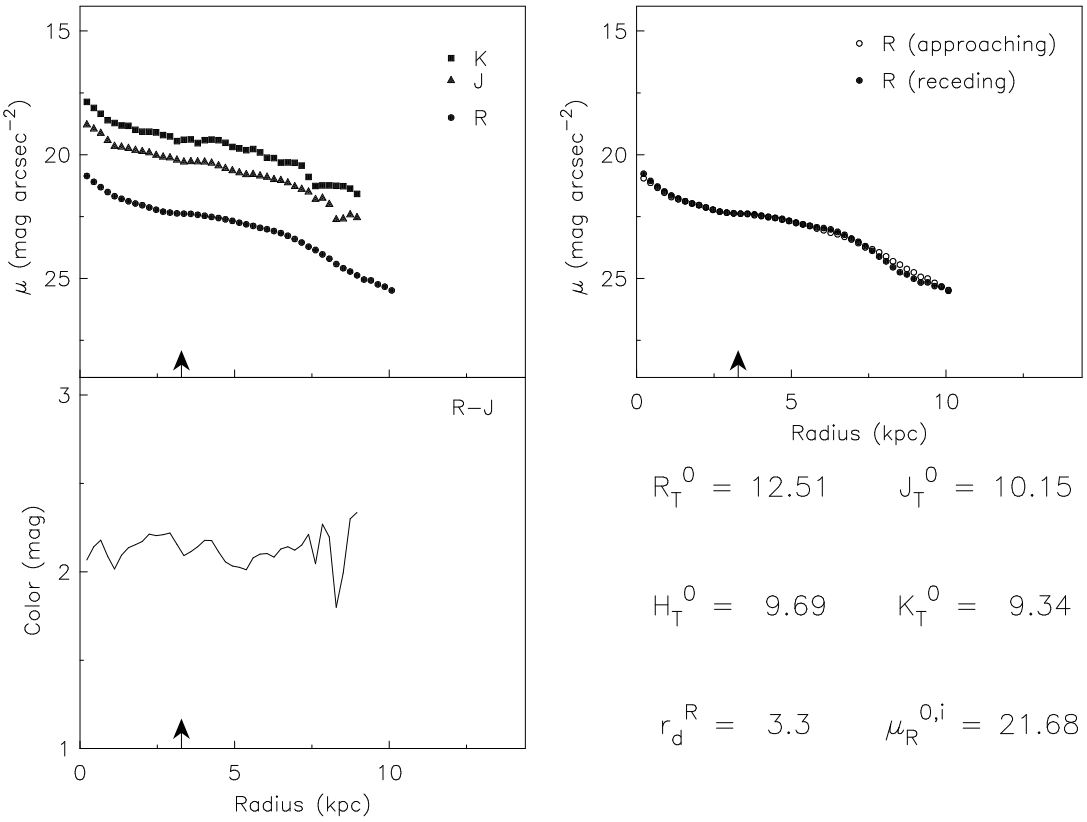

$R_T^0 = 12.51$ $J_T^0 = 10.15$

$H_T^0 = 9.69$ $K_T^0 = 9.34$

$r_d^R = 3.3$ $\mu_R^{0,i} = 21.68$

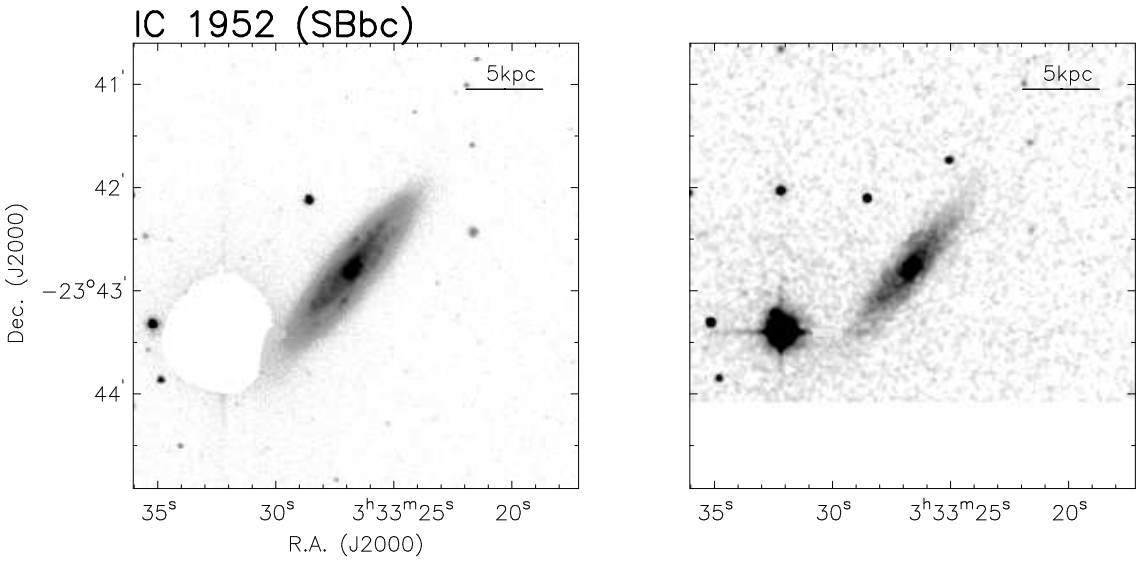

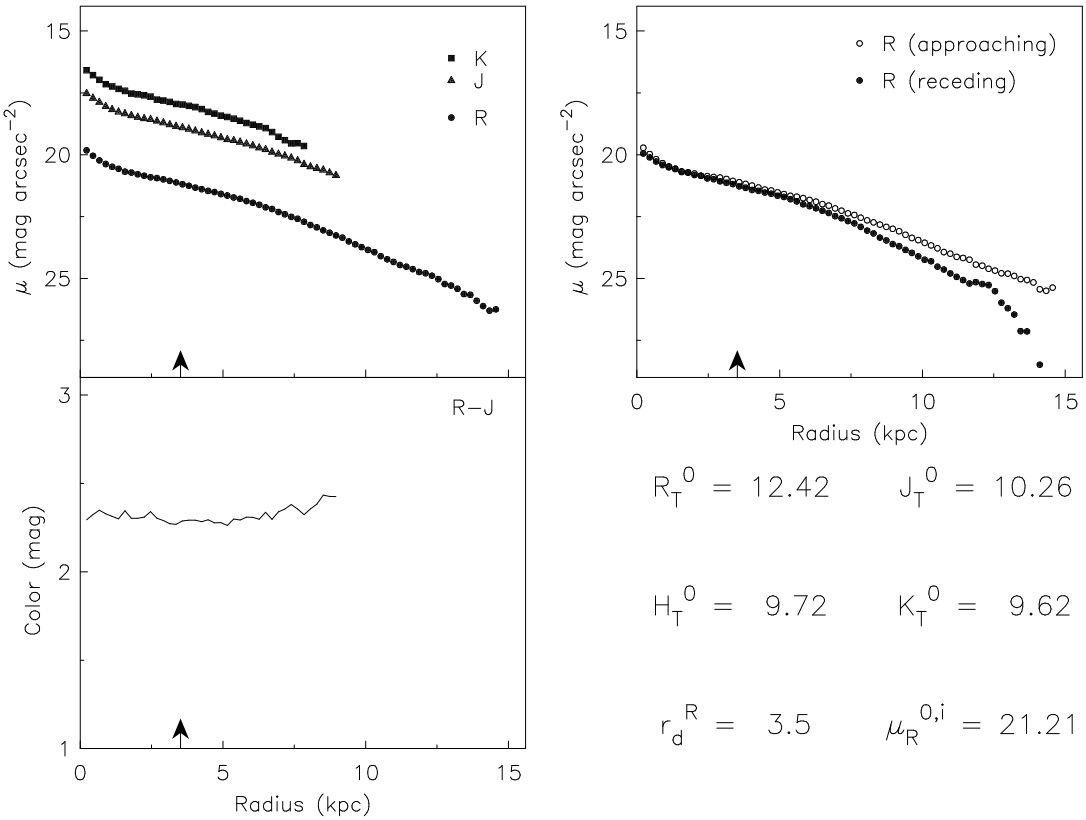

$R_T^0 = 12.42$ $J_T^0 = 10.26$

$H_T^0 = 9.72$ $K_T^0 = 9.62$

$r_d^R = 3.5$ $\mu_R^{0,i} = 21.21$

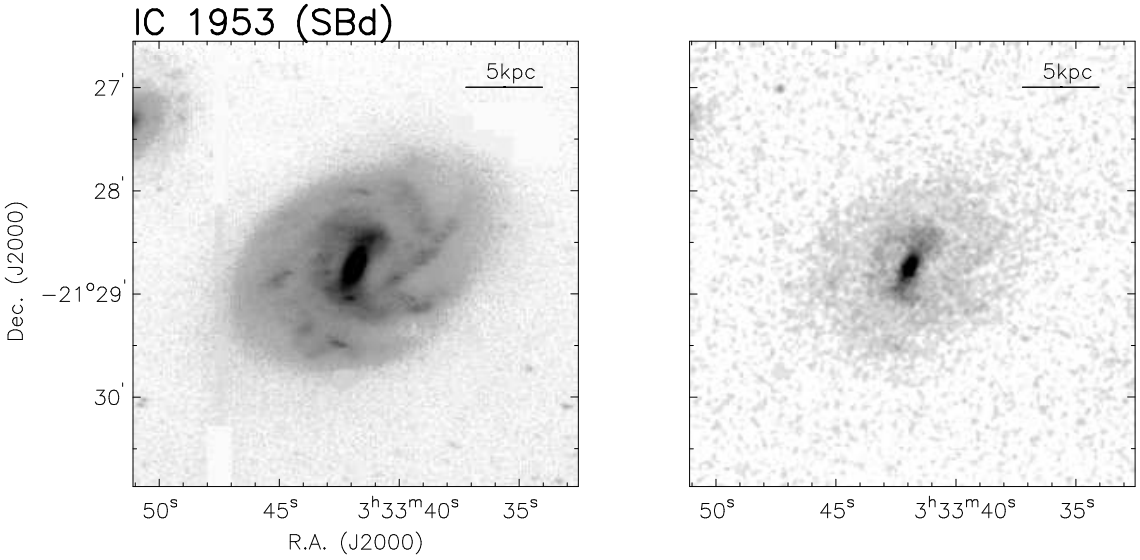

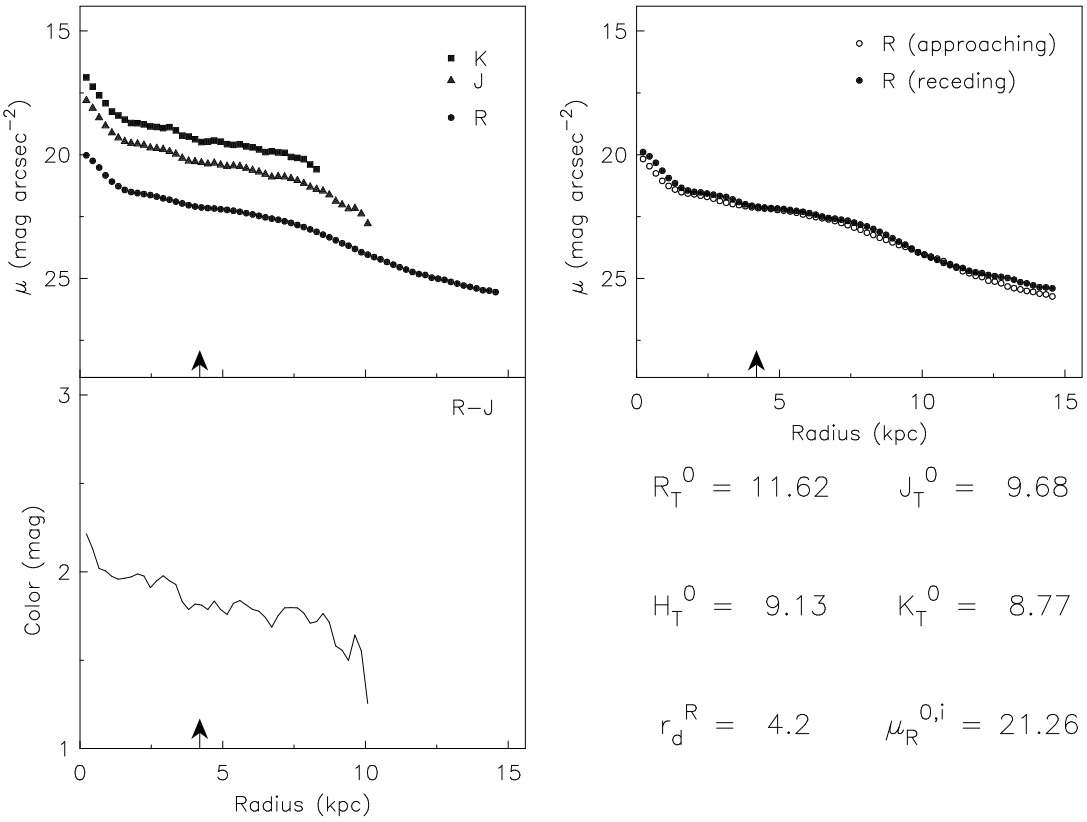

$R_T^0 = 11.62$ $J_T^0 = 9.68$

$H_T^0 = 9.13$ $K_T^0 = 8.77$

$r_d^R = 4.2$ $\mu_R^{0,i} = 21.26$

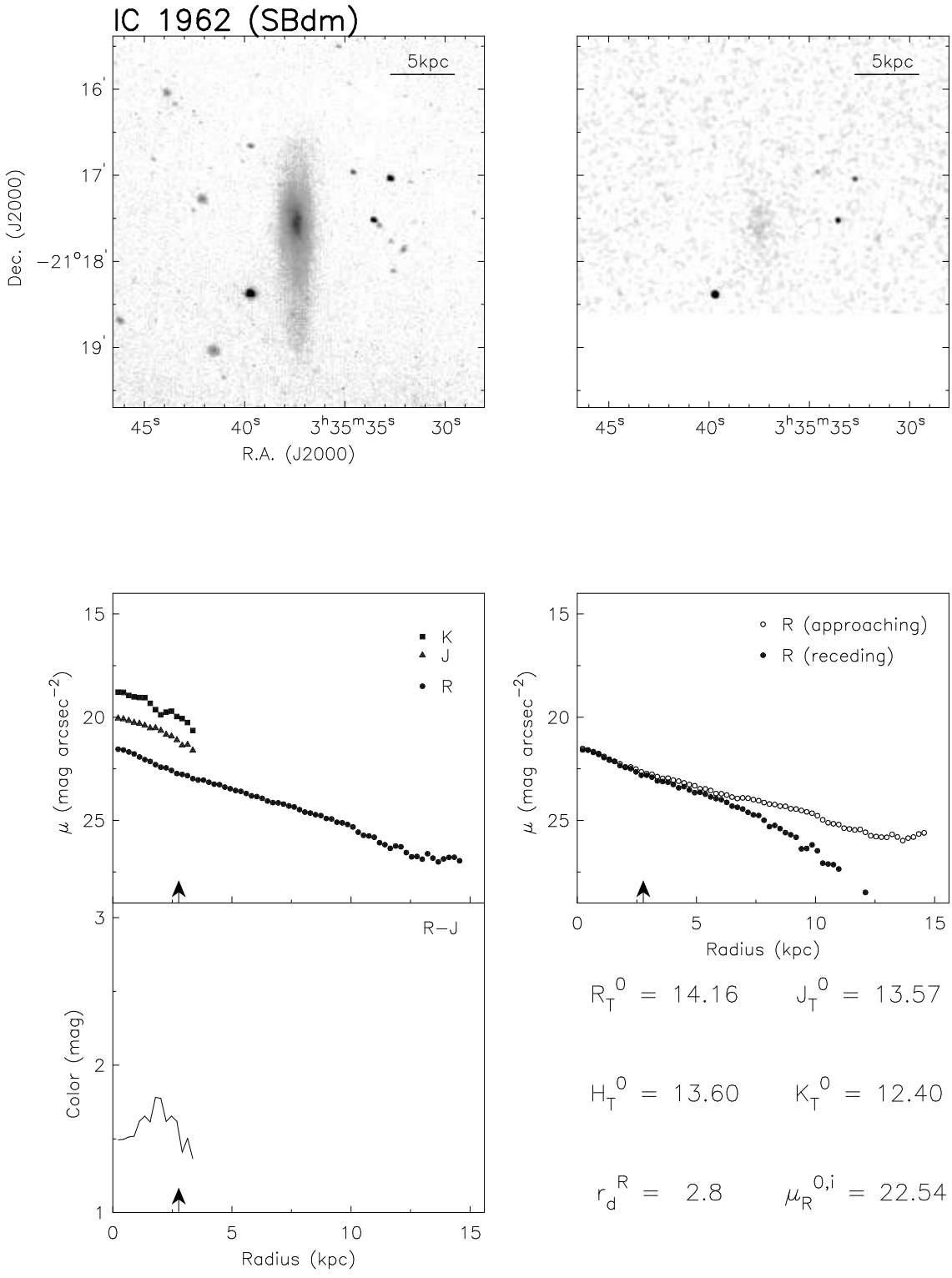

$R_T^0 = 14.16$ $J_T^0 = 13.57$

$H_T^0 = 13.60$ $K_T^0 = 12.40$

$r_d^R = 2.8$ $\mu_R^{0,i} = 22.54$

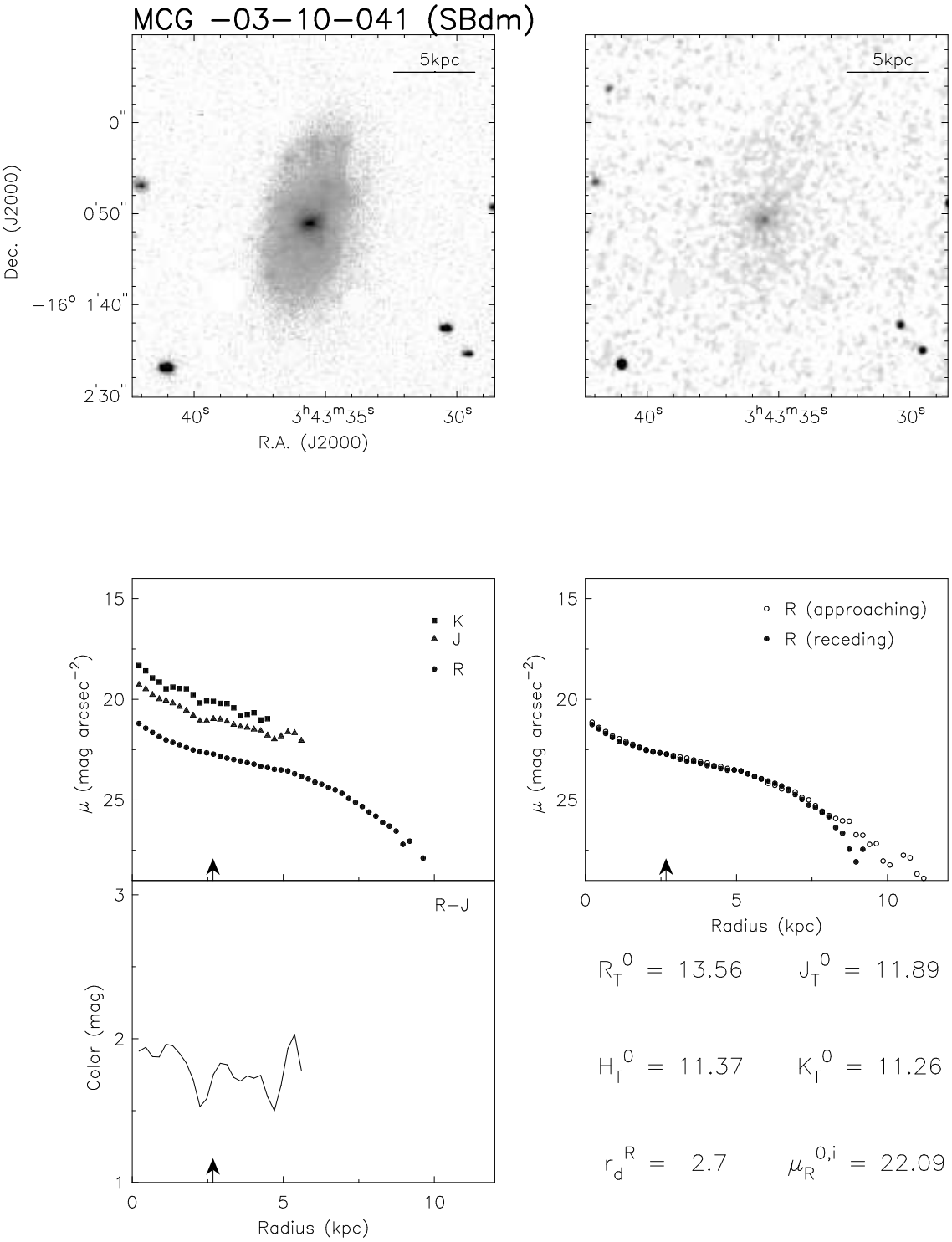
MCG −03−10−041 (SBdm)
5kpc
5kpc
Dec. (J2000)
0″
0′50″
−16° 1′40″
2′30″
40s
3h43m35s
30s
R.A. (J2000)
μ (mag arcsec−2)
K
J
R
R−J
Color (mag)
Radius (kpc)
R (approaching)
R (receding)
R_T^0 = 13.56
J_T^0 = 11.89
H_T^0 = 11.37
K_T^0 = 11.26
r_d^R = 2.7
$\mu_R^{0,i}$ = 22.09

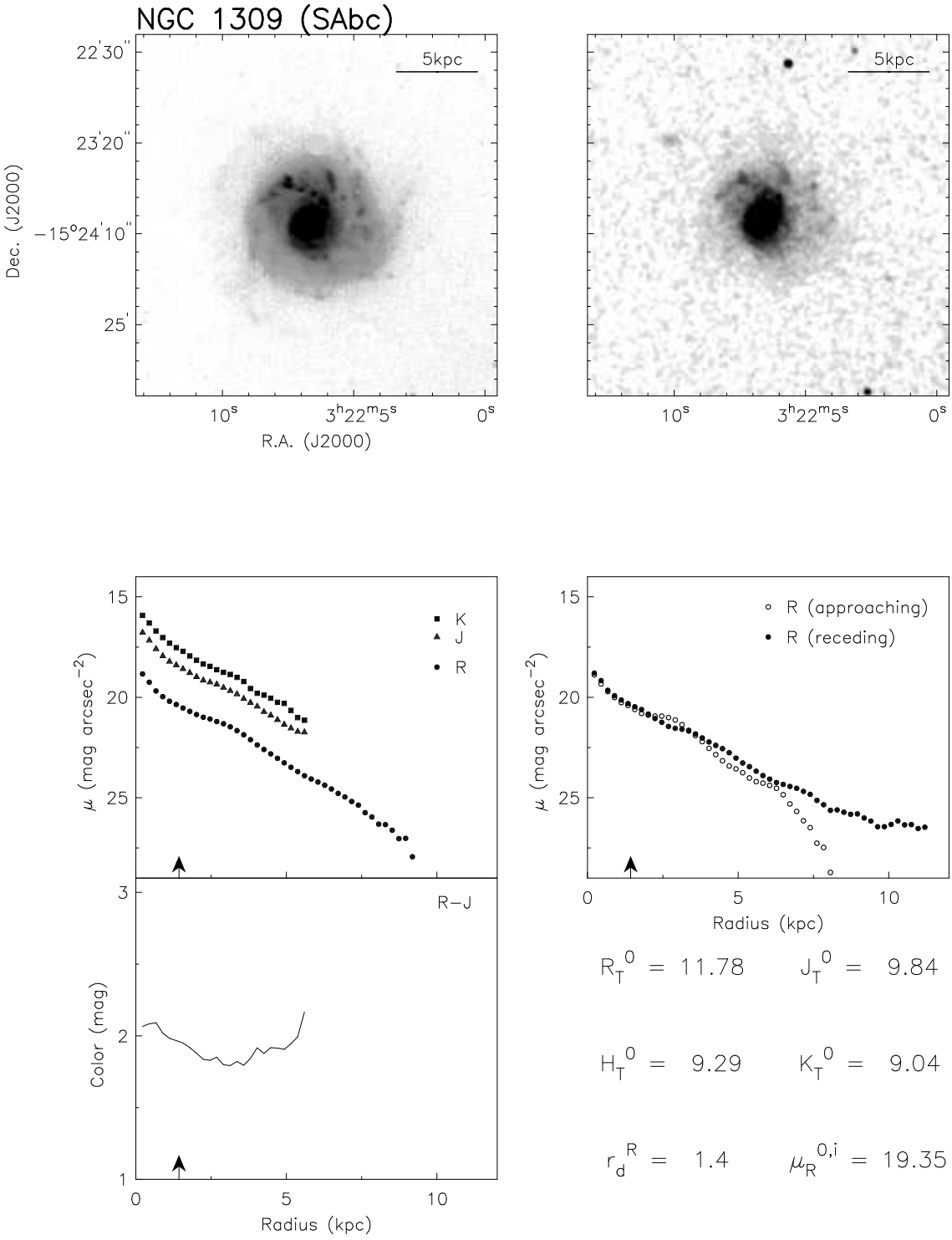

$R_T^0 = 11.78$ $J_T^0 = 9.84$

$H_T^0 = 9.29$ $K_T^0 = 9.04$

$r_d^R = 1.4$ $\mu_R^{0,i} = 19.35$

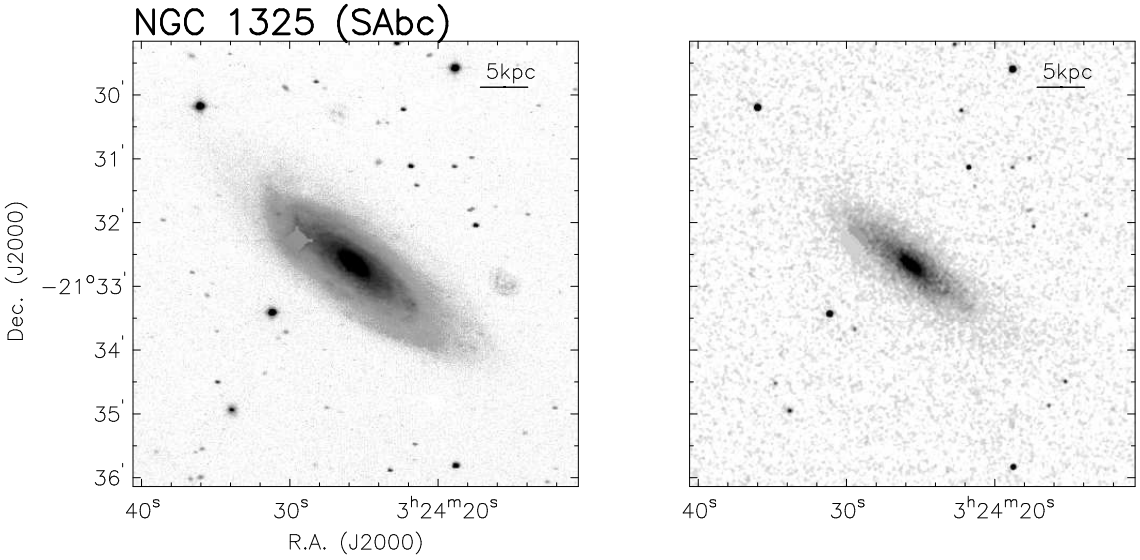

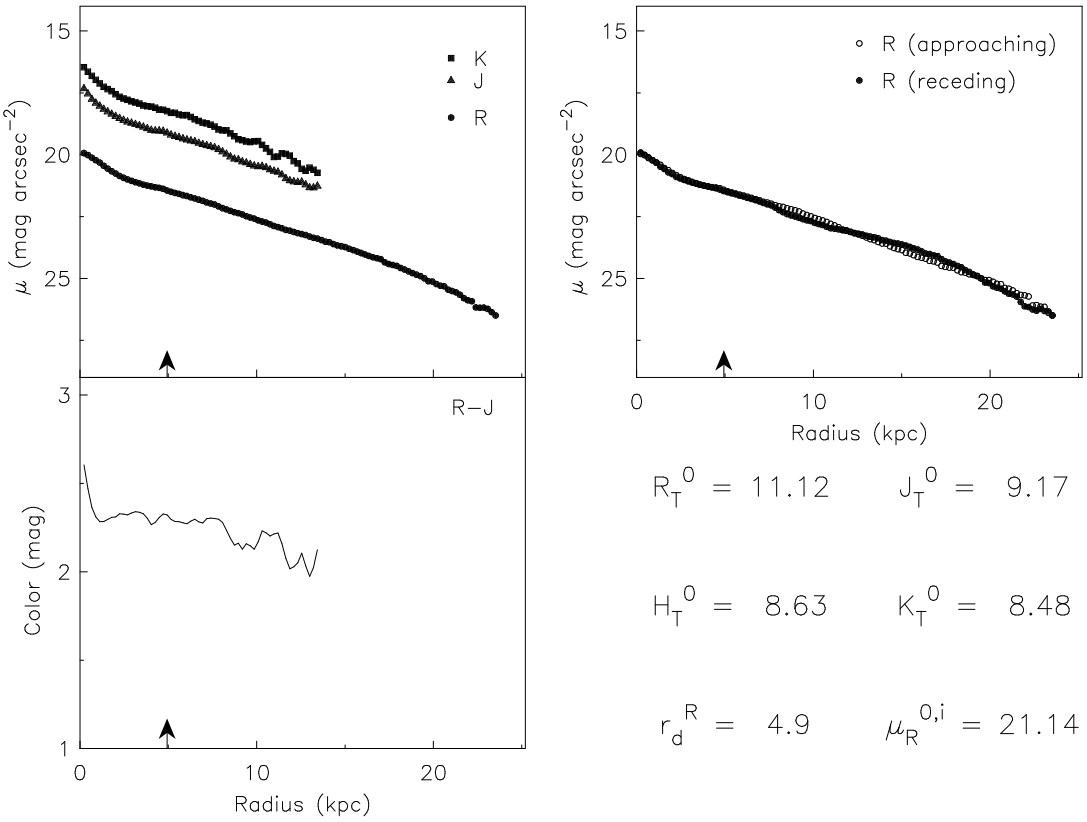

$R_T^0 = 11.12$ $J_T^0 = 9.17$

$H_T^0 = 8.63$ $K_T^0 = 8.48$

$r_d^R = 4.9$ $\mu_R^{0,i} = 21.14$

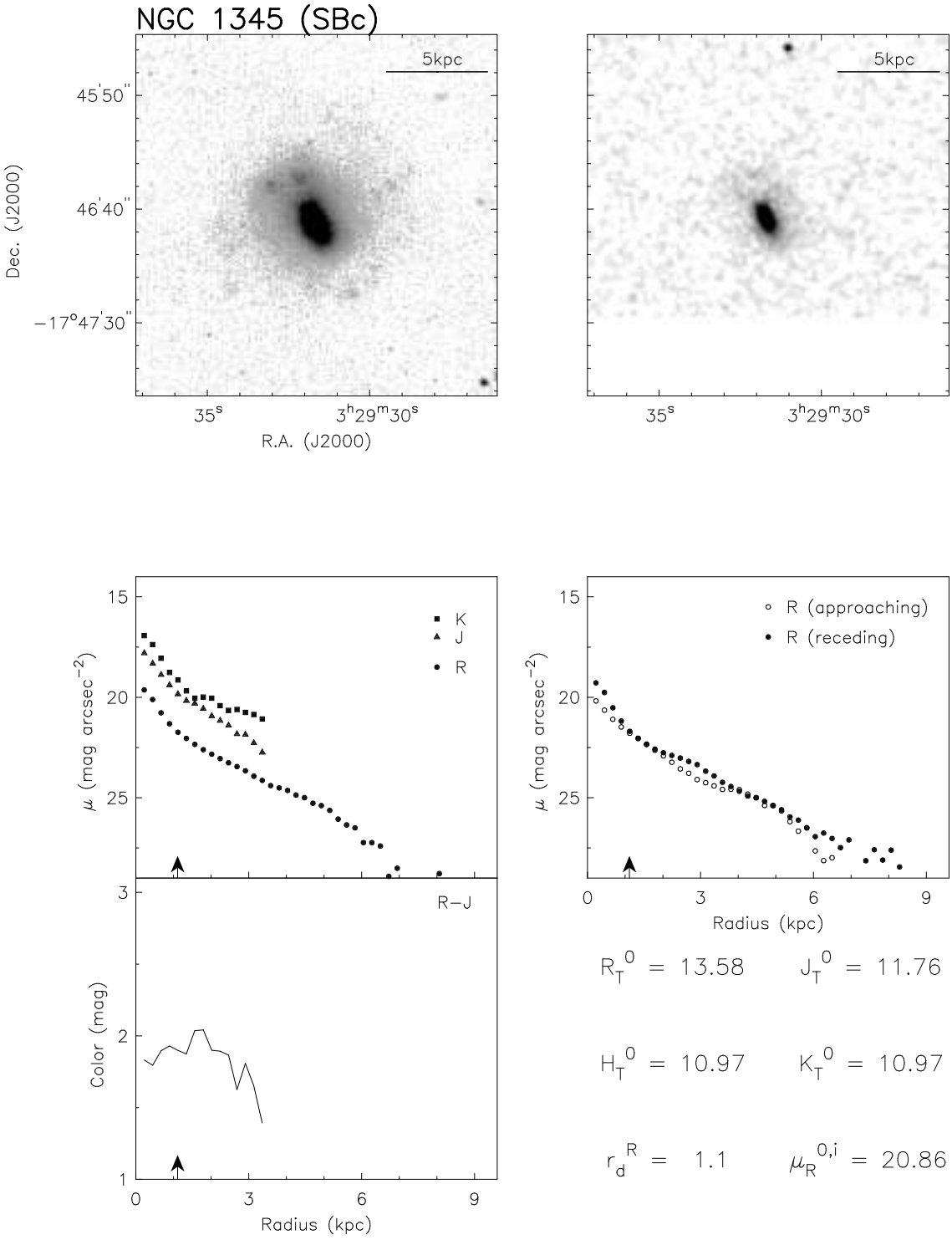

$R_T^0 = 13.58$ $J_T^0 = 11.76$

$H_T^0 = 10.97$ $K_T^0 = 10.97$

$r_d^R = 1.1$ $\mu_R^{0,i} = 20.86$

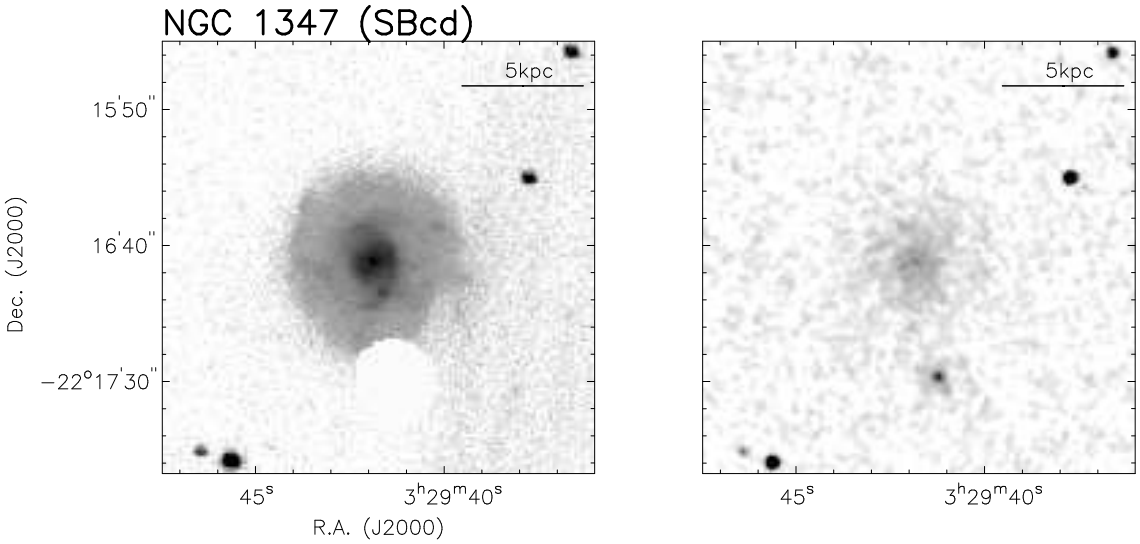

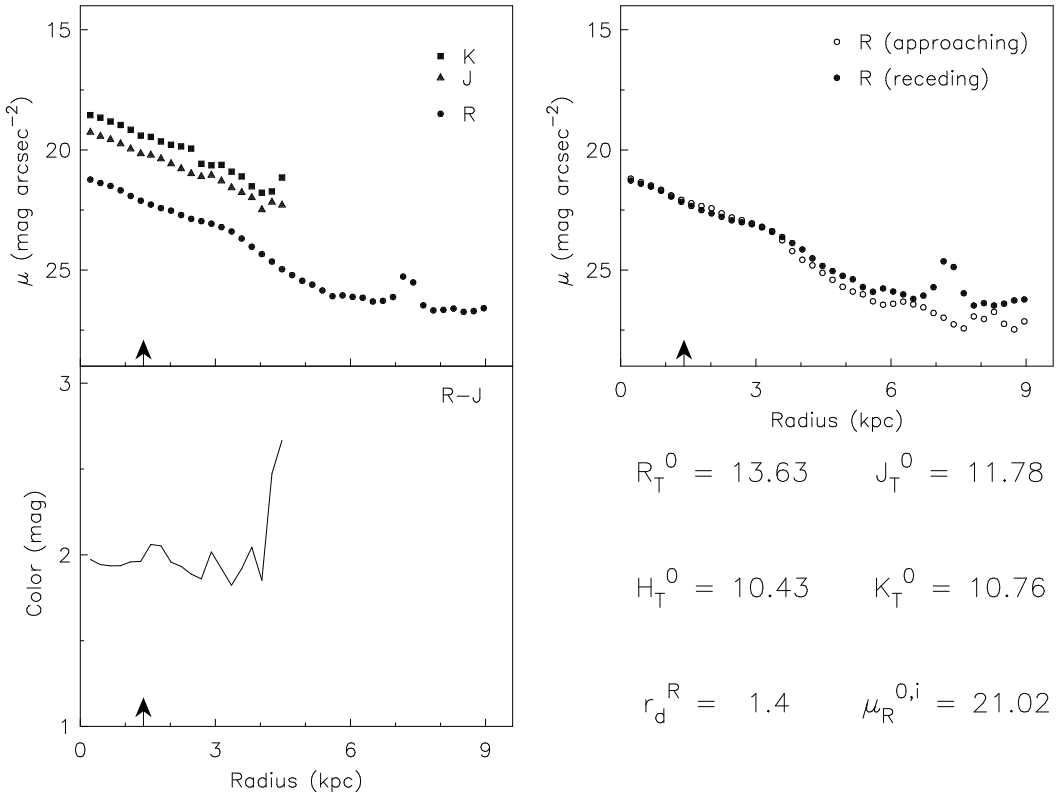

$R_T^0 = 13.63$ $J_T^0 = 11.78$

$H_T^0 = 10.43$ $K_T^0 = 10.76$

$r_d^R = 1.4$ $\mu_R^{0,i} = 21.02$

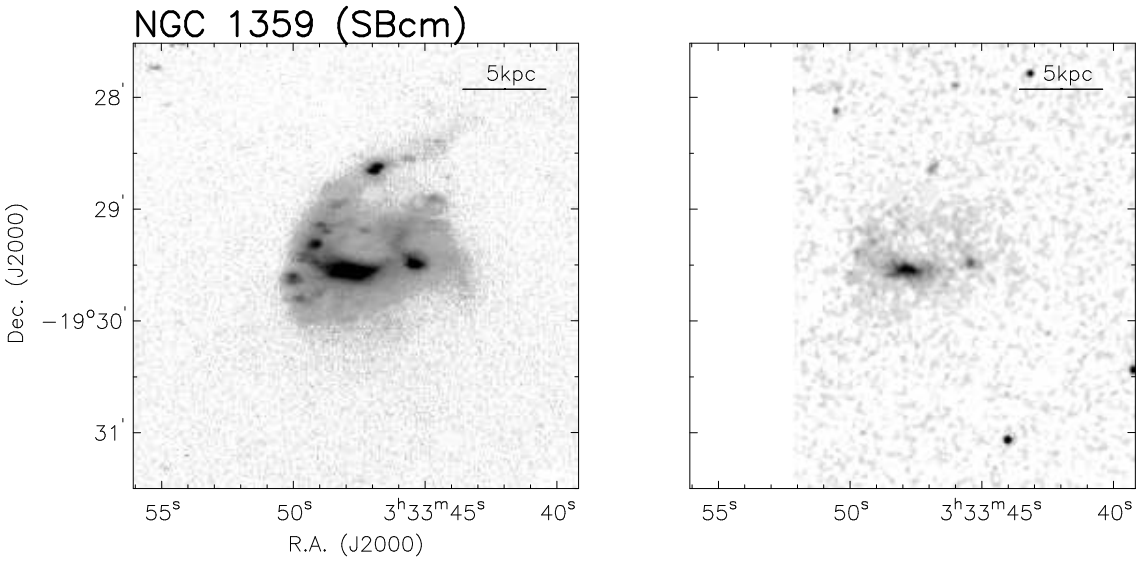

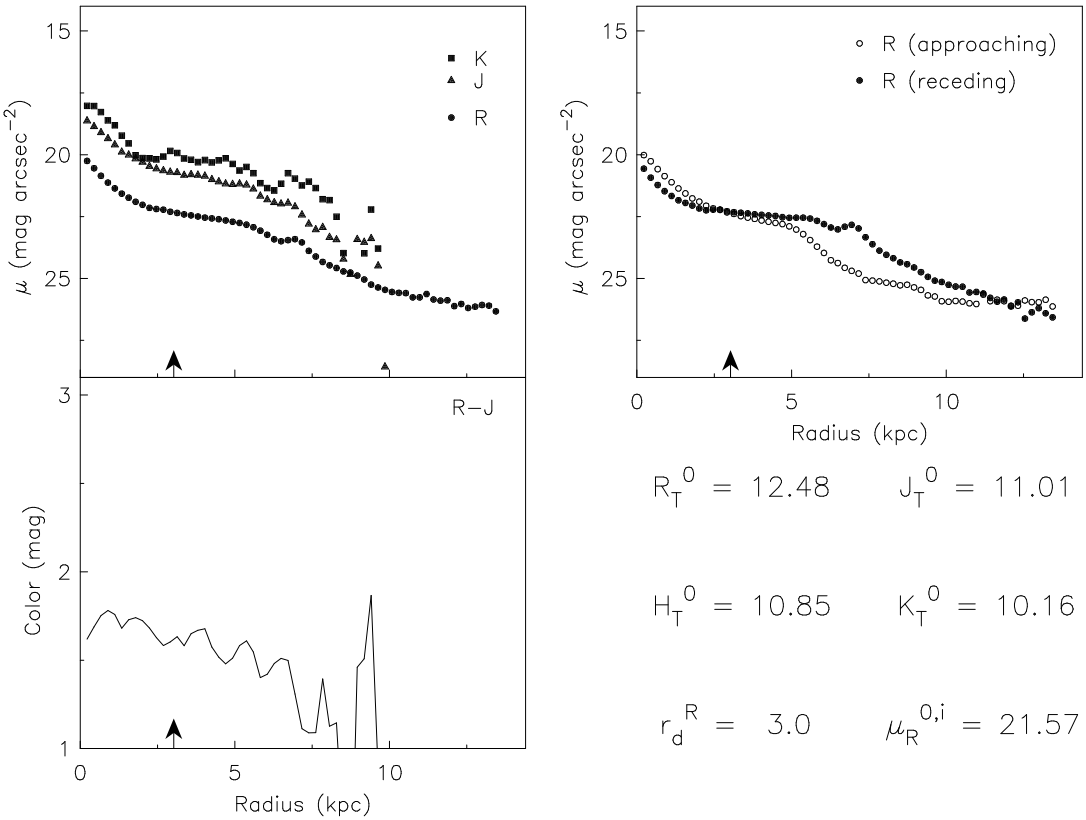

$R_T^0 = 12.48$ $J_T^0 = 11.01$

$H_T^0 = 10.85$ $K_T^0 = 10.16$

$r_d^R = 3.0$ $\mu_R^{0,i} = 21.57$

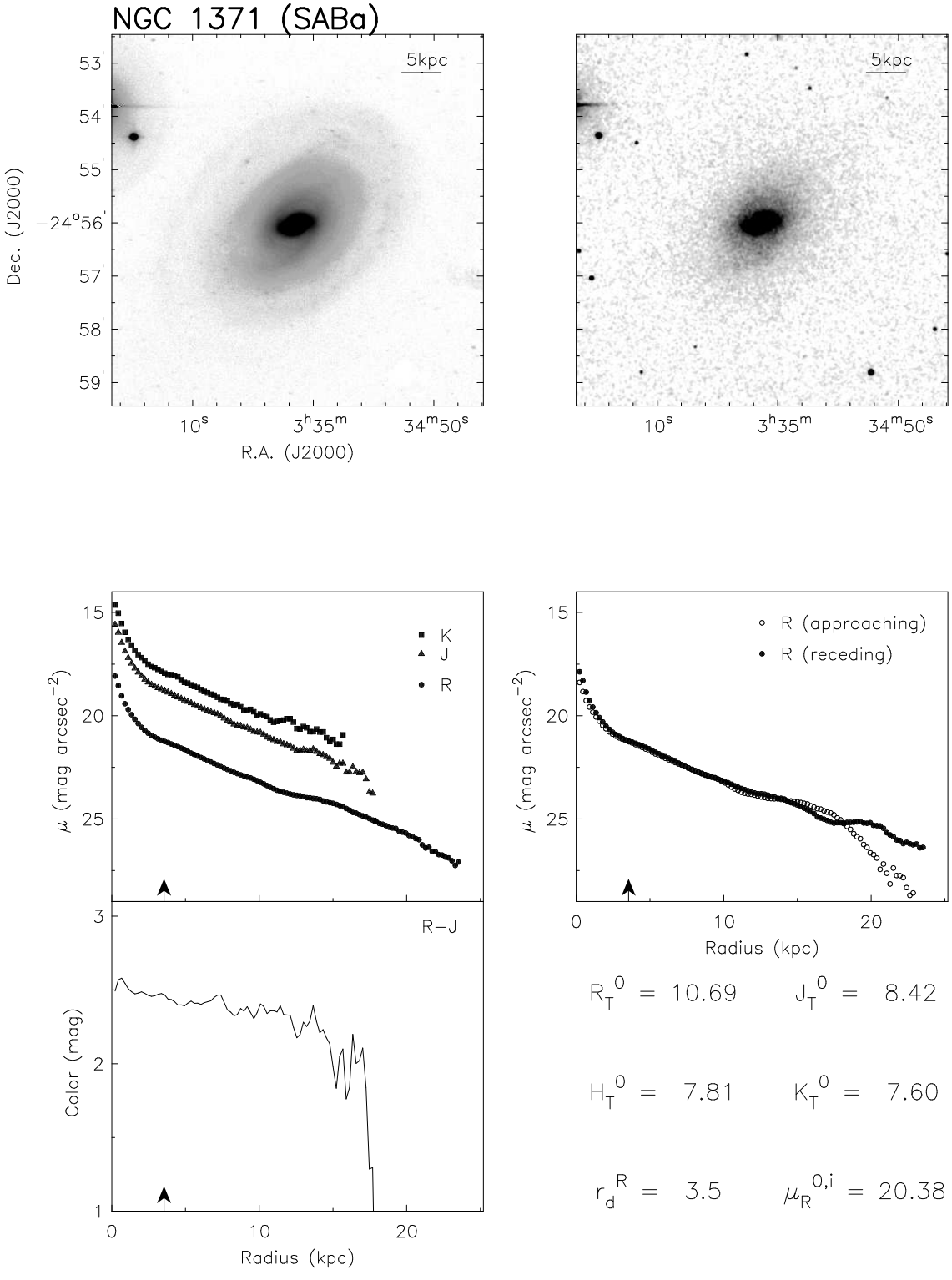
NGC 1371 (SABa)
5kpc
Dec. (J2000)
R.A. (J2000)
10^s
3^h35^m
34^m50^s
$-24°56'$
53'
54'
55'
57'
58'
59'
μ (mag arcsec^{-2})
K
J
R
R−J
Color (mag)
Radius (kpc)
R (approaching)
R (receding)
R_T^0 = 10.69
J_T^0 = 8.42
H_T^0 = 7.81
K_T^0 = 7.60
r_d^R = 3.5
$\mu_R^{0,i}$ = 20.38

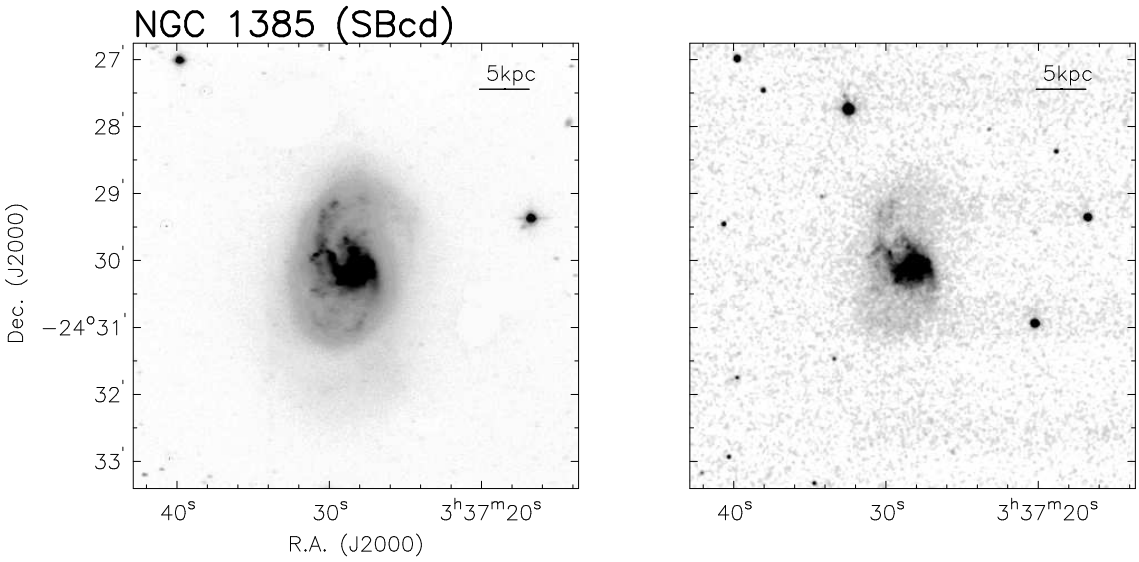

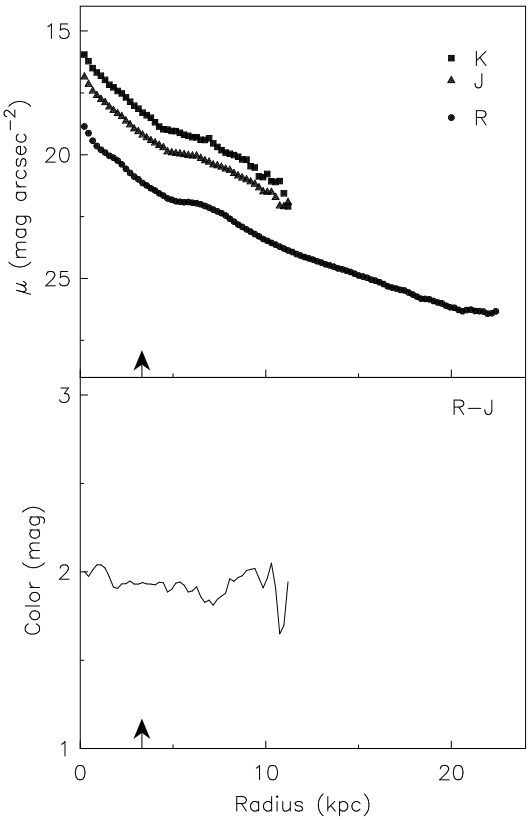

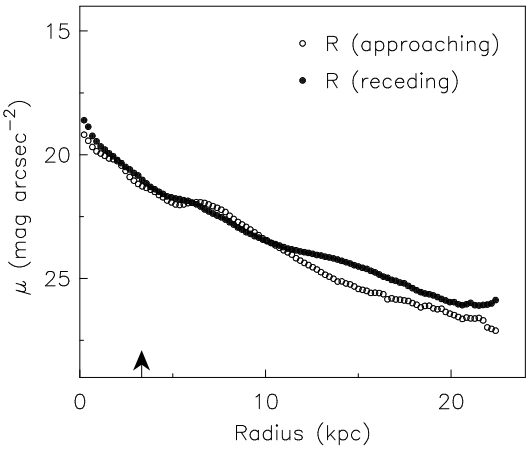

$R_T^0 = 10.84$ $J_T^0 = 9.02$

$H_T^0 = 8.40$ $K_T^0 = 8.26$

$r_d^R = 3.3$ $\mu_R^{0,i} = 20.42$

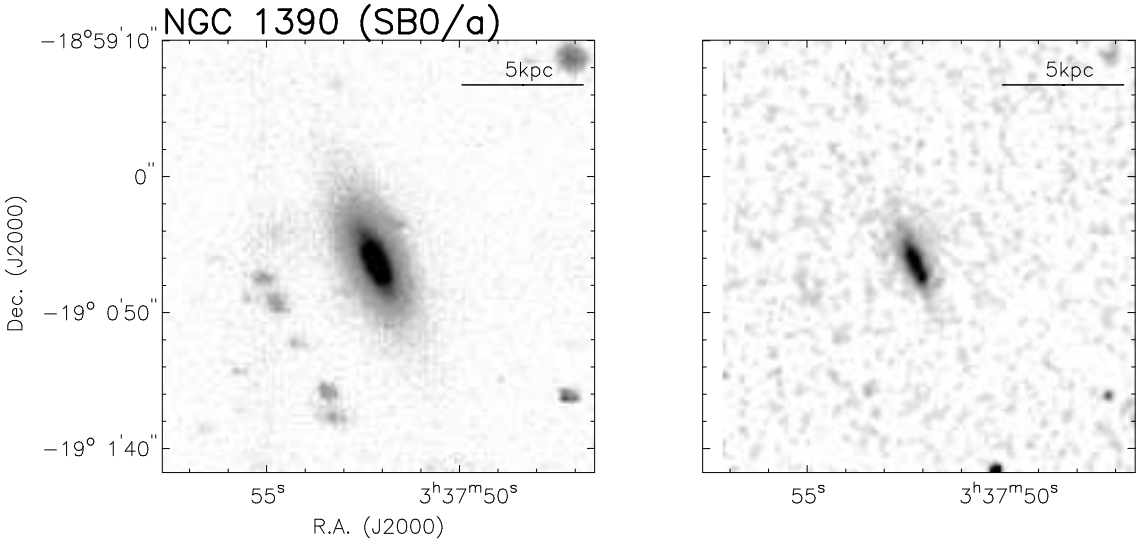

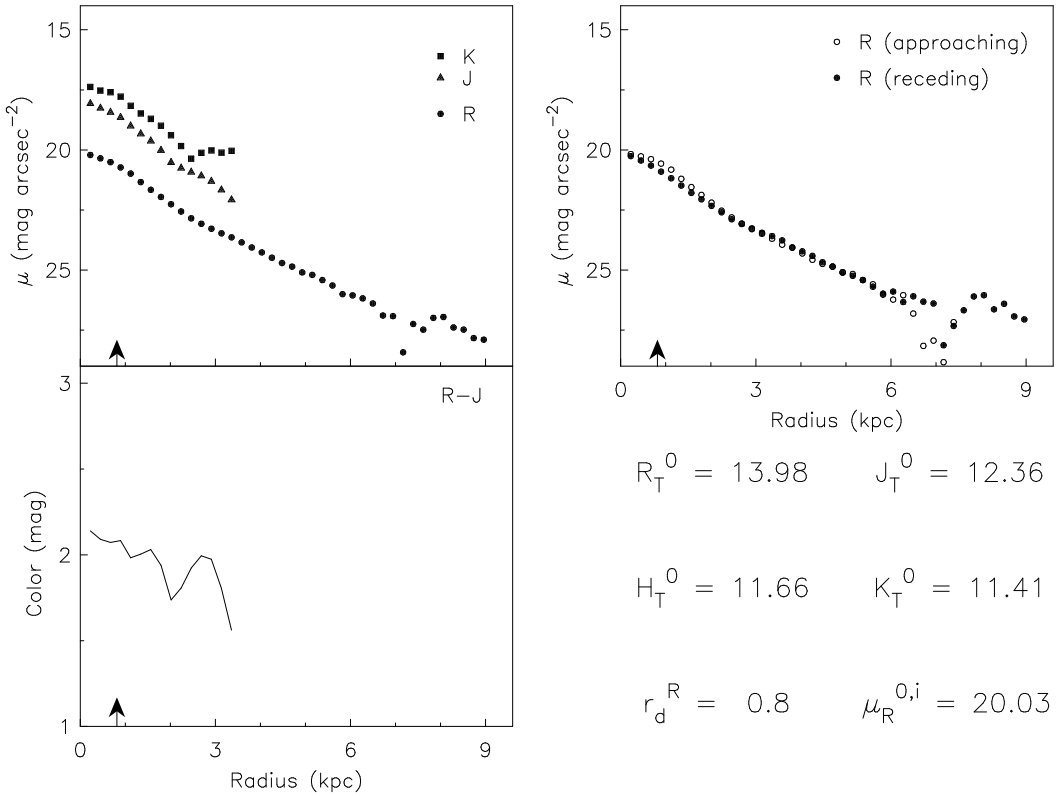

$R_T^0 = 13.98$ $J_T^0 = 12.36$

$H_T^0 = 11.66$ $K_T^0 = 11.41$

$r_d^R = 0.8$ $\mu_R^{0,i} = 20.03$

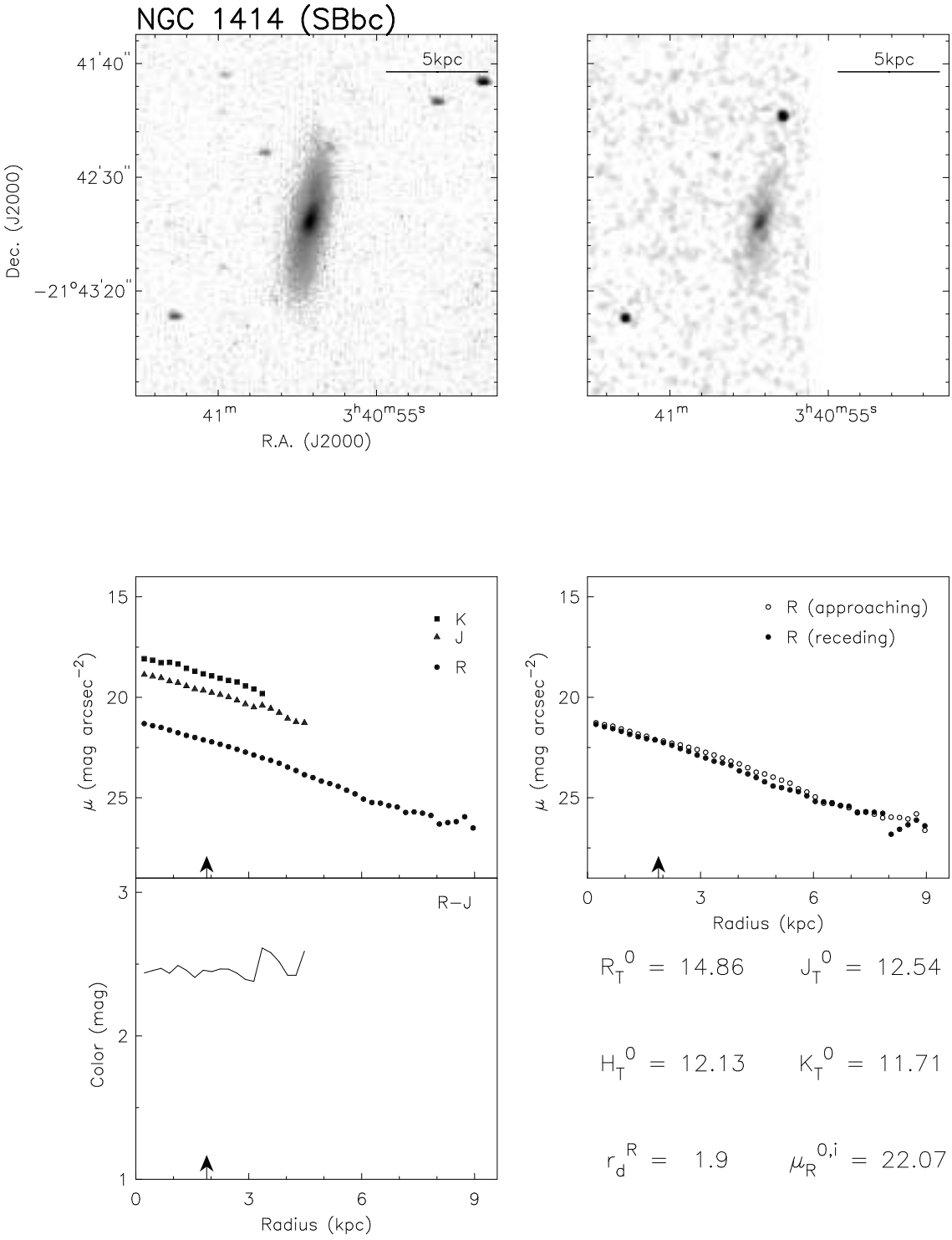
NGC 1414 (SBbc)
5kpc
41'40"
42'30"
−21°43'20"
Dec. (J2000)
41^m
3^h40^m55^s
R.A. (J2000)
5kpc
41^m
3^h40^m55^s
15
20
25
μ (mag arcsec^−2)
K
J
R
R−J
3
2
1
Color (mag)
0
3
6
9
Radius (kpc)
R (approaching)
R (receding)
15
20
25
μ (mag arcsec^−2)
0
3
6
9
Radius (kpc)
R_T^0 = 14.86
J_T^0 = 12.54
H_T^0 = 12.13
K_T^0 = 11.71
r_d^R = 1.9
μ_R^0,i = 22.07

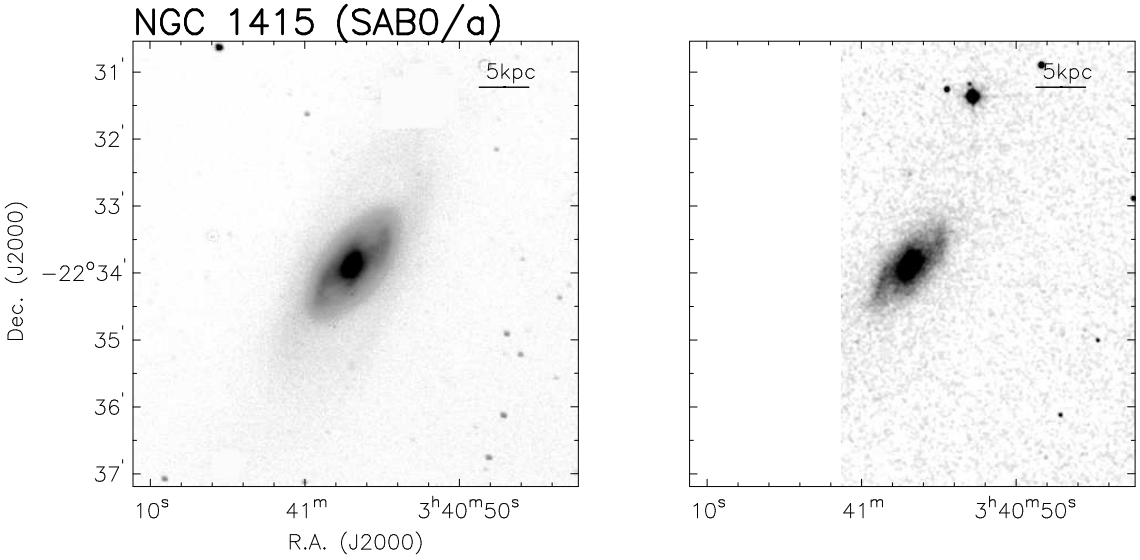

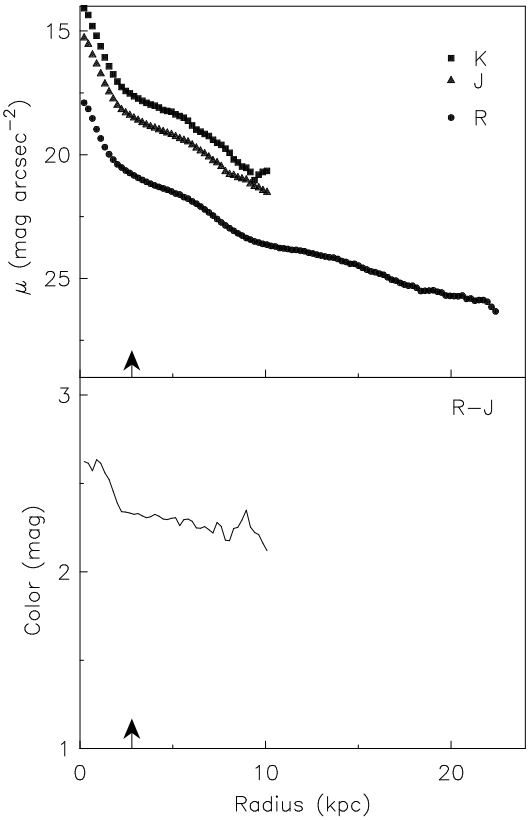

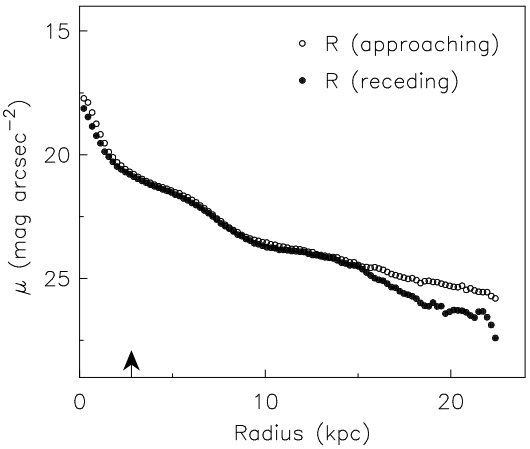

$R_T^0 = 11.05$ $J_T^0 = 8.99$

$H_T^0 = 8.44$ $K_T^0 = 8.17$

$r_d^R = 2.8$ $\mu_R^{0,i} = 20.26$

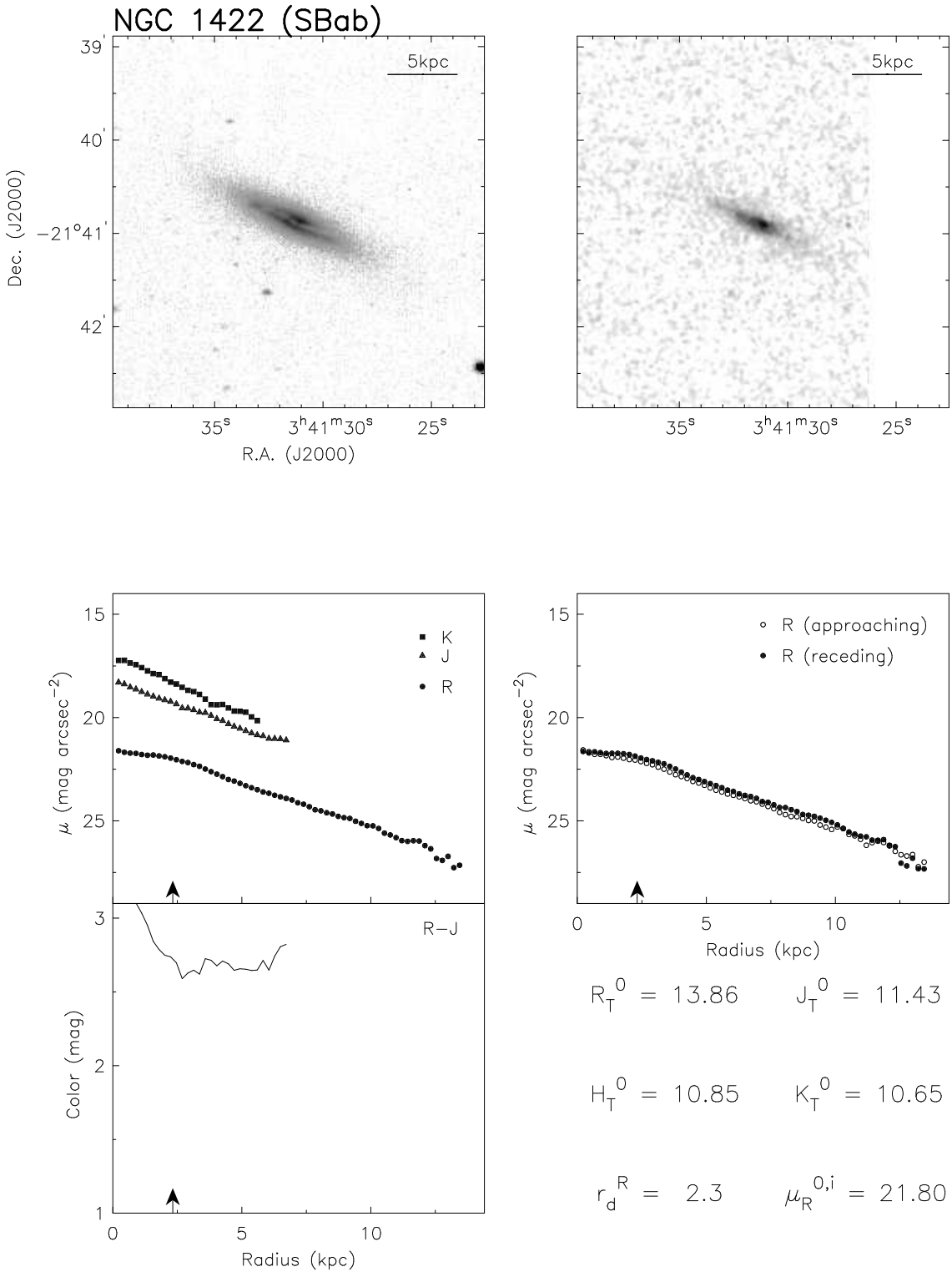

$R_T^0 = 13.86$ $J_T^0 = 11.43$

$H_T^0 = 10.85$ $K_T^0 = 10.65$

$r_d^R = 2.3$ $\mu_R^{0,i} = 21.80$

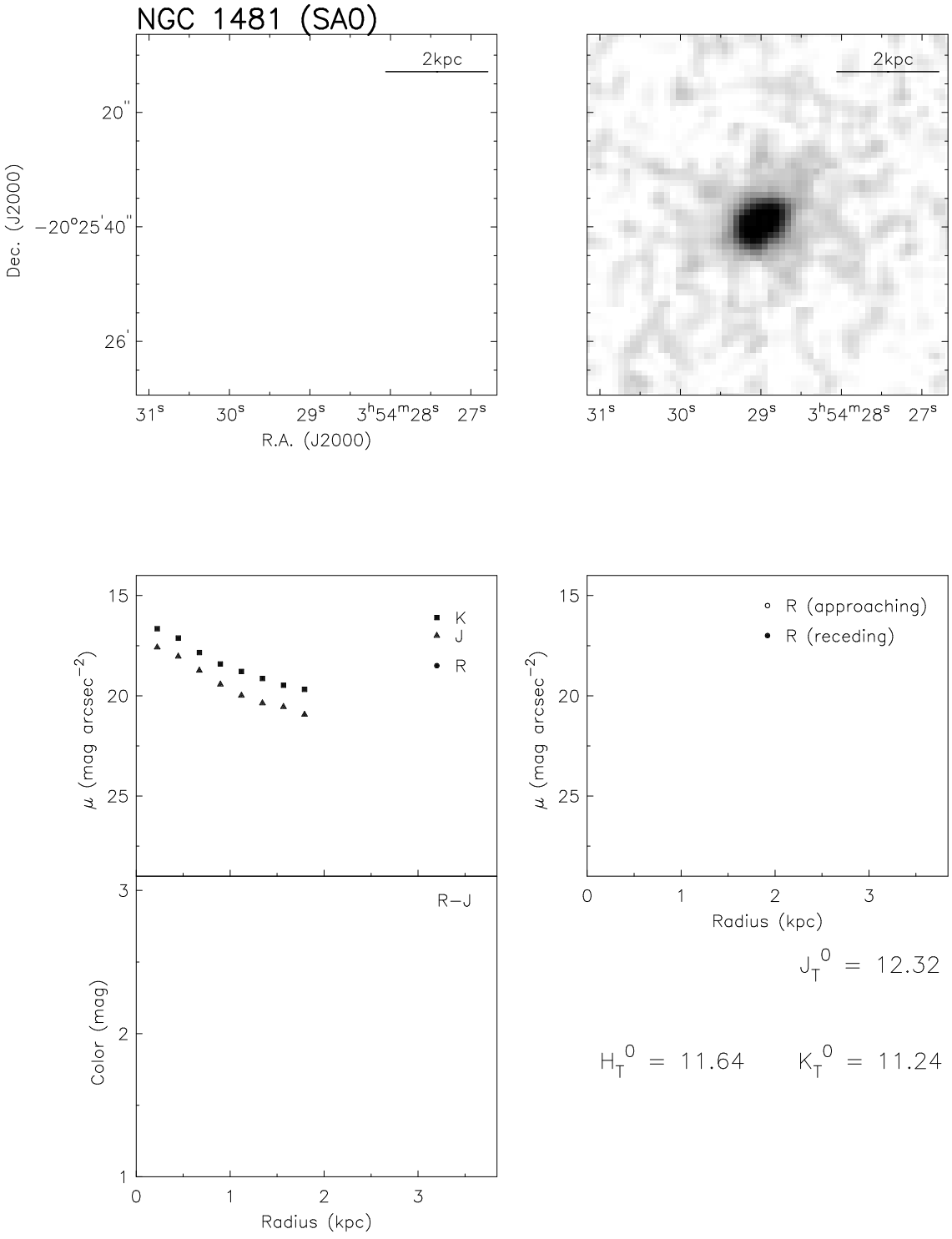
NGC 1481 (SA0)
2kpc
20"
−20°25'40"
26'
Dec. (J2000)
31s
30s
29s
3h54m28s
27s
R.A. (J2000)
2kpc
31s
30s
29s
3h54m28s
27s
15
20
25
μ (mag arcsec−2)
K
J
R
R−J
3
2
1
Color (mag)
0
1
2
3
Radius (kpc)
R (approaching)
R (receding)
15
20
25
μ (mag arcsec−2)
0
1
2
3
Radius (kpc)
J_T^0 = 12.32
H_T^0 = 11.64
K_T^0 = 11.24

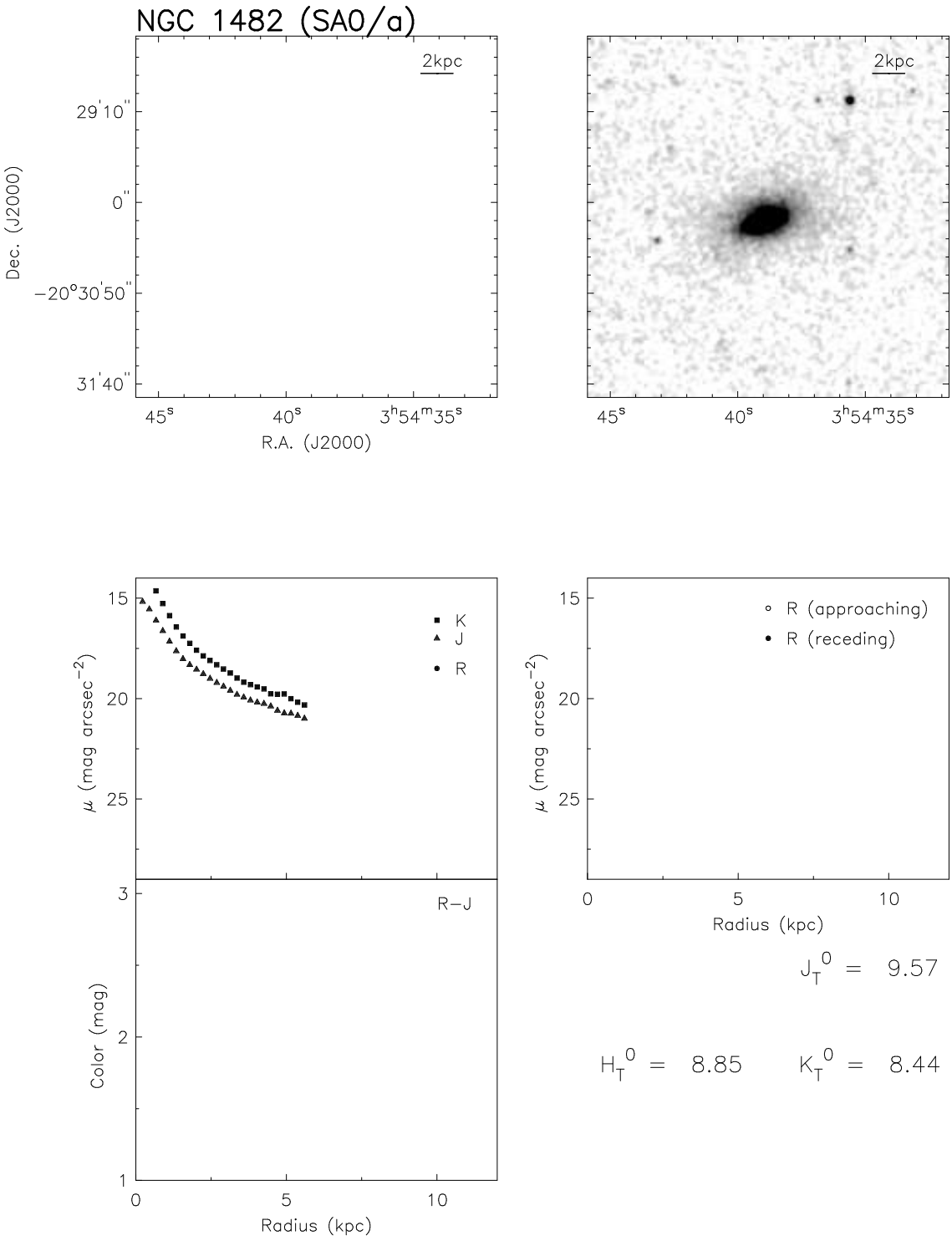
NGC 1482 (SA0/a)
2kpc
29'10"
0"
−20°30'50"
31'40"
Dec. (J2000)
45s
40s
3h54m35s
R.A. (J2000)
2kpc
45s
40s
3h54m35s
15
20
25
μ (mag arcsec−2)
K
J
R
R−J
3
2
1
Color (mag)
0
5
10
Radius (kpc)
R (approaching)
R (receding)
15
20
25
μ (mag arcsec−2)
0
5
10
Radius (kpc)
J_T^0 = 9.57
H_T^0 = 8.85
K_T^0 = 8.44

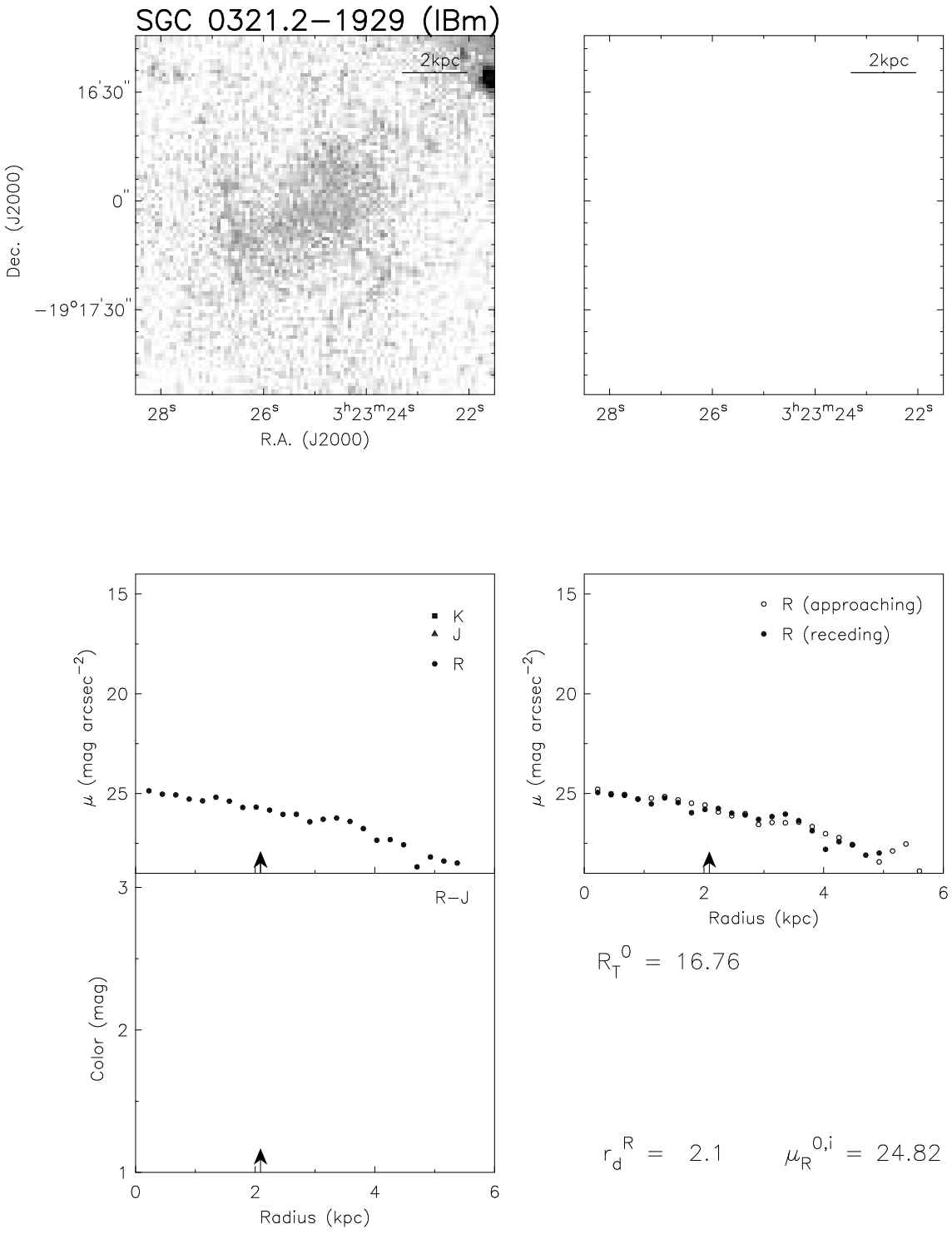

$R_T^0 = 16.76$

$r_d^R = 2.1$ $\mu_R^{0,i} = 24.82$

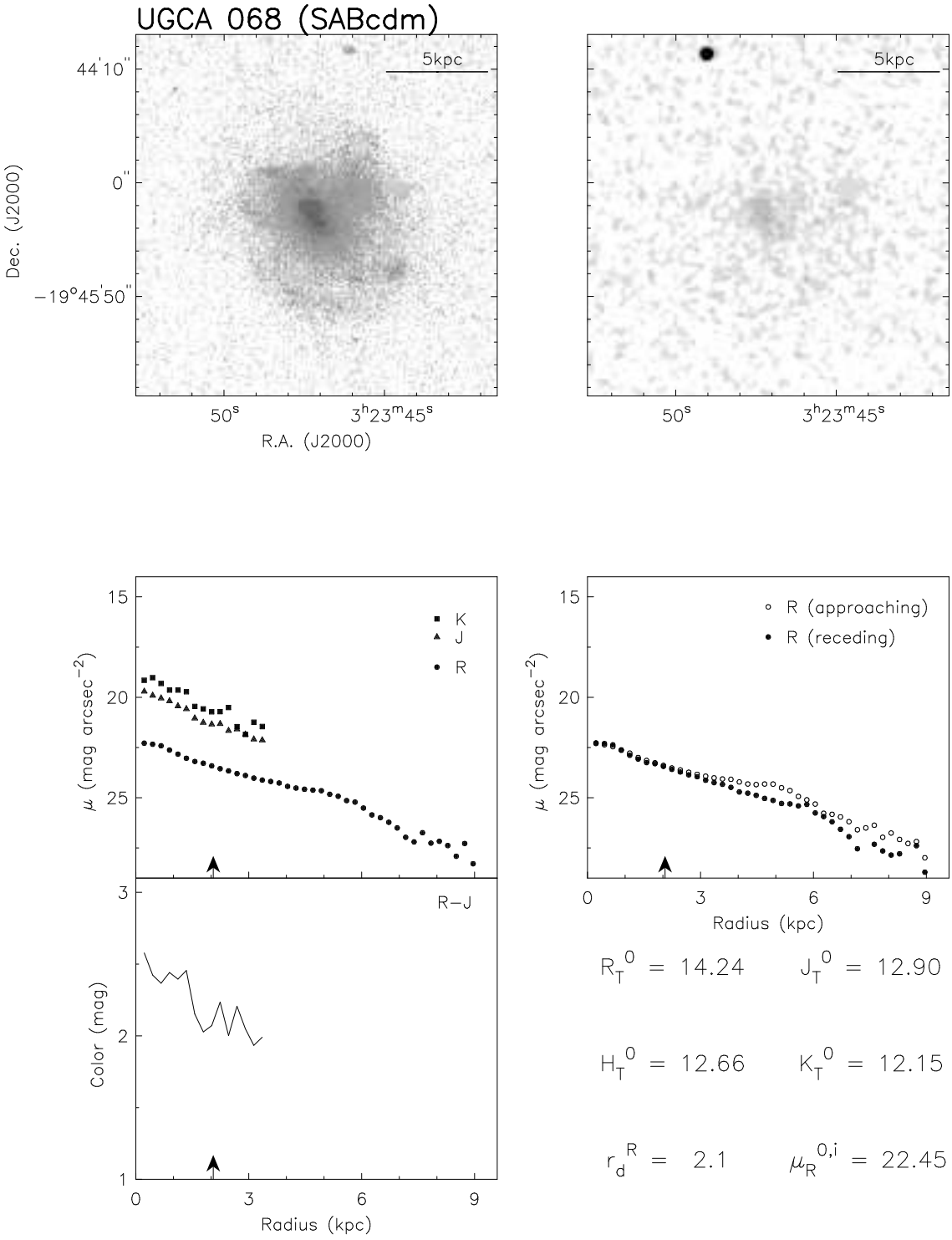

$R_T^0 = 14.24$ $J_T^0 = 12.90$

$H_T^0 = 12.66$ $K_T^0 = 12.15$

$r_d^R = 2.1$ $\mu_R^{0,i} = 22.45$

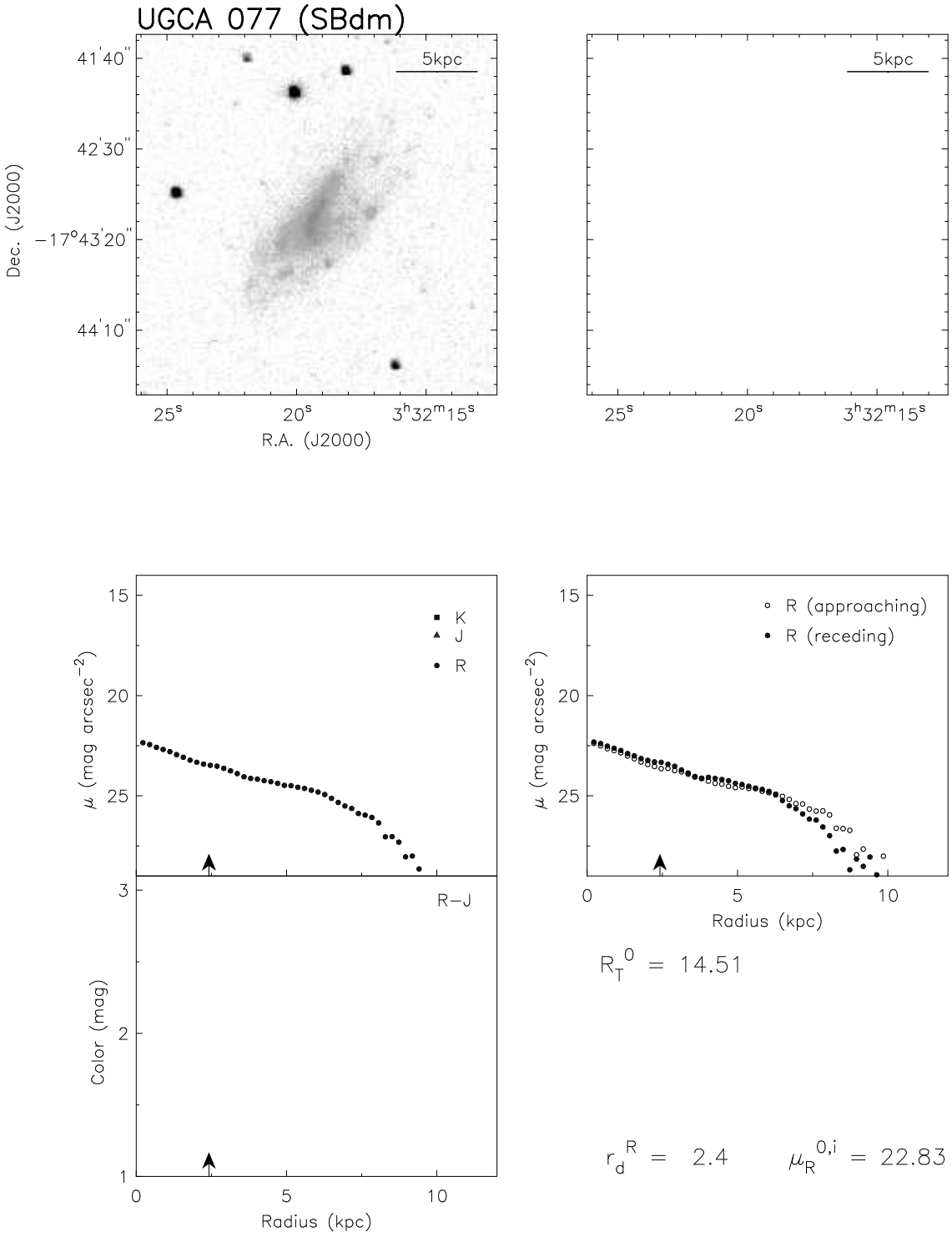
UGCA 077 (SBdm)
5kpc
41'40"
42'30"
−17°43'20"
44'10"
Dec. (J2000)
25s
20s
3h32m15s
R.A. (J2000)
5kpc
25s
20s
3h32m15s
15
20
25
μ (mag arcsec−2)
K
J
R
R−J
3
2
1
Color (mag)
0
5
10
Radius (kpc)
R (approaching)
R (receding)
15
20
25
μ (mag arcsec−2)
0
5
10
Radius (kpc)
R_T^0 = 14.51
r_d^R = 2.4
μ_R^0,i = 22.83